Electrochemical Reduction of Furfural-based Biomass Intermediates

By

John James Roylance

A dissertation submitted in partial fulfillment of
the requirements for the degree of

Doctor of Philosophy

(Chemistry)

at the

UNIVERSITY OF WISCONSIN–MADISON

2016

Date of final oral examination: 06/13/2016

The dissertation is approved by the following members of the Final Oral Committee:

Kyoung-Shin Choi, Professor, Chemistry
John F. Berry, Professor, Chemistry
Ronald T. Raines, Professor, Biochemistry
Clark Landis, Professor, Chemistry
Ive Hermans, Associate Professor, Chemistry

Abstract

In the quest for more renewable and sustainable fuels and chemical feedstocks, 5-hydroxymethylfurfural (HMF) has emerged as one of the most promising compounds, being processed into important fuels, chemical building blocks, and pharmaceutical compounds, among others. Much of HMF's marketable potential has yet to be explored and remains untapped, leading to it being dubbed one of the "Sleeping Giants" of the chemical industry. Current methods of HMF reduction require use of high temperatures and pressures of H_2, or other useful sacrificial reagents. Reduction of HMF in much more mild conditions with readily abundant sources of hydrogen, such as water, could help lower the cost of HMF processing and drive its utilization in the market as a green chemistry reagent.

The work presented herein explores the use of electrochemical methods for the reduction of HMF and other furfural-based biomass intermediates using water as the source of hydrogen. By controlling parameters such as electrode material and morphology, pH, electrolyte composition, and applied potential, fine control over electrochemical reduction processes and products is achieved with efficiencies and selectivities approaching 100%. Furthermore, combining solar energy conversion and biomass conversion by direct utilization of photogenerated charge carriers for HMF reduction would decrease processing costs even further. Pairing the catalyst cathode to a $BiVO_4$ photoanode under 1 sun illumination decreases the external bias required by more than half and results in photoelectrochemical reduction of HMF at high efficiencies with no sacrificial reagents. These results will help to further establish biomass as a viable and sustainable alternative to fossil fuels for our fuel and commodity chemical needs.

Acknowledgments

It is only with the love, support, and sacrifice of countless individuals that I have been able to get to this point and accomplish this great task. I have been shaped, molded, and influenced by family, friends, neighbors, and teachers over the years. It would be impossible to identify and acknowledge all who have aided me in my life journey, but there are a few of particular importance whom I would like to thank.

First of all, thank you to my dear angel wife, Sara. You were with me through good and bad, sickness and health. You helped me bring 5 beautiful and amazing children into this world. You sacrificed and gave of yourself day after day and night after night. You did this joyfully and with the hope of a glorious and beautiful future together. This glorious and beautiful future will happen, I have that faith and hope, but it will have to wait for a season. You were taken from me too soon and won't get to appreciate the fruits of our labor in this mortal life, but there is most certainly a glorious and beautiful future for us when at last I am called home to come join you. I love you and miss you, my dear. I could not have accomplished this without you. Even without you by my side this past year, your influence has forever changed me and inspired me to persevere through all trials and challenges. Thank you.

Thank you to my mother and father who have lived their lives in sacrifice and service to others. You have taught me some of the most important lessons I have learned including the importance of hard work, determination, honesty and integrity. You also taught me the importance of love, faith, and hope. Without these, especially faith and hope, getting to this point would have been insurmountable. I will forever be indebted to you for helping me after Sara passed away. I would not have been able to finish my work without your selfless service.

If I work diligently all my days to improve myself and become a better man and become half the measure of a person each of you are, I will have accomplished something truly great and will have become a remarkable person. I cannot thank you enough or think more highly of you.

To the rest of my large and wonderful family, thank you for your love and support. The baby of the family has grown up and accomplished something greater than you probably ever imagined I could, and much of it is thanks to you. I looked to your examples of discipline and determination, but also joy and happiness, as I grew and developed into the man I am today. You will certainly inspire in the years to come as well. Also, thank you for your love and support this past year as I have had to rediscover my path in the wake of Sara's passing.

To Dr. Choi, in a very real sense I could not have done this without you! Thank you for taking a chance on me, both at Purdue and with the transfer to UW-Madison, and for your kindness and patience all these years. Also, thank you for all of the time and energy you invested in teaching and training me. You taught me many invaluable lessons pertaining to the sciences and to life in general. I will forever be in your debt. I am grateful that we have had opportunities to get to know each other on a professional level as well as a personal level. May your future be filled with joy and success!

Thank you to the rest of my committee members. Thank you Dr. Raines and Dr. Berry for the guidance over the years, and Dr. Raines also for the inspiration to work on this subject matter. Thank you Dr. Landis and Dr. Hermans for agreeing to be on my committee and for your wonderful questions and insight.

Thank you to all of the Choi group members, past and present, from Purdue and UW-Madison. You have entertained me through the long days, encouraged me through difficult

times, and inspired me to work harder. You have taught me and helped me to become a better scientist, and I hope to have done the same for you.

I owe much of the success of this past year to the good and loving people of my local church congregation, the Madison 2nd Ward. There is absolutely no way I could have survived this last year with my health or sanity or the health and wellbeing of my children without your loving assistance. You helped love and care for my children in Sara's absence and made it possible for me to complete this work. Thank you. You will forever and always be dear to my heart.

Last, but most important of all, I need to thank my God, my great Heavenly Father, who gave me life and limb, and all that I am and have. I love you more than I can ever express. I thank my Lord and Savior, Jesus Christ, who walked with me and often carried me through my trials and heartache. You were there with me, my truest friend and confidant, as I mourned the loss of my dear Sara, and raised me up to be able to finish this task and move on in life. Thank you, thank you, thank you.

Table of Contents

Chapter 1. Introduction to Biomass Conversion and Electrochemical Organic Synthesis

1.1. Introduction

Since the dawn of the industrial revolution man has been dependent upon fossil fuels for heating, electricity, and transportation needs, as well as for the production of numerous consumer goods from plastics to pharmaceuticals.[1,2] As a result, there have been ever increasing levels of atmospheric CO_2 and concerns have arisen over the sustainability of our current and projected energy demands while maintaining a fossil fuel economy.[3,4] There is now approximately 1 teraton of excess CO_2 in the atmosphere compared to pre-industrial revolution levels.[5] Therefore, these problems give rise to two particular areas of interest. First, establishing an efficient, reliable, and sustainable pathway to provide energy and commodity chemicals is necessary. Second, developing an efficient and practical route to convert the potentially harmful excess CO_2 in our atmosphere to useful products is of great importance. The first area was the driving force behind research done at UW-Madison and is the focus of chapters 2-4. The second area was the focus for research conducted during my first two years of graduate school while at Purdue University and will be addressed in greater detail in chapter 5.

Biomass, a naturally renewable and sustainable source of organic carbon, has become an important alternative to fossil fuels. Cellulosic matter (cellulose and hemicelluloses) is the most abundant organic material on earth.[6,7] It comprises anywhere from more than half to more than three quarters of biomass, with cellulose being the major component.[1] Cellulose is a polysaccharide, or sugar polymer, formed by repeated glucose monomers.[6,7] It forms long, crystalline sheets due to repeating bond patterns and hydrogen bonds between parallel chains.[6,7] Starch, another polymer of glucose, has a branched, amorphous nature due to variations in the bonds between glucose monomers.[1] Hemicellulose is a polysaccharide composed of several different sugars (xylose, arabinose, galactose, glucose, and mannose) and is largely substituted

with acetic acid, also leading to a branched, amorphous nature.[1,2] While there is an abundant supply of this useful material, fossil fuels continue to be the main source of chemicals and fuels because cellulosic matter requires significant processing to be fully utilized. These polysaccharides are broken down into their respective monomers by hydrolysis of the glycosidic bond. The branched natures of starch and hemicellulose result in much easier hydrolysis.[1,2] In the case of starch this unfortunately means utilizing material commonly used as food for other purposes (e.g. using corn to produce ethanol for fuel-additive purposes), and the numerous sugars in hemicellulose makes separation difficult and time consuming.[8] Since humans are unable to digest cellulose and it is composed of only glucose, it seems to be the most promising biomass source to pursue.

1.2. A Way Forward with Biomass

The various pentoses (five-carbon sugars) and hexoses (six-carbon sugars) derived from hydrolysis of cellulosic matter can be processed into numerous biomass intermediates and chemical building blocks.[2,9] One of the most pursued biomass intermediates is 5-hydroxymethylfurfural (HMF). HMF is produced from the dehydration of hexoses, most predominantly fructose and glucose, though recent work has been done to streamline the process of converting raw cellulosic matter to HMF.[2,10,11] HMF can be undergo oxidation, reduction, and etherification to numerous chemicals and value added products.[2,4,9-19] The versatility of HMF and scope to which it can be utilized for fuels and building block chemistry has led to it being considered among the top 10 biomass-based platform chemicals by the US Department of Energy.[12] The result of HMF reduction yields two chemicals which have been of particular interest (Figure 1.1), 2,5-bis(hydroxymethyl)furan (BHMF), which can be utilized for bioplastics and biodiesel, and 2,5-dimethylfuran (DMF), which is a potential fuel or fuel additive.

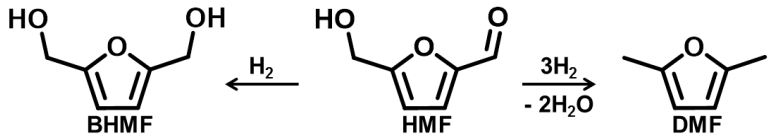

Figure 1.1. Reduction of HMF to BHMF or DMF using H_2 as the hydrogen source.

BHMF is produced by reduction of the formyl (aldehyde) group of HMF. It is water soluble, has a much higher boiling point than HMF (275 °C vs. 115 °C) and undergoes polymerization or etherification to industrially important compounds such as polyester, polyurethane foams and biodiesel.[4,15,20,21] Reduction of HMF to BHMF is commonly achieved using one of three different methods. The first method utilizes $NaBH_4$ as the reducing agent and hydrogen source in cooled (277 K) dry methanol for 15 minutes,[20] or ethanol at room temperature for 12 hours.[21] Another conversion method utilizes cooled formalin (283 K), which is an aqueous solution of formaldehyde, and 17 M sodium hydroxide. In the presence of base, formaldehyde and HMF undergo a crossed Cannizzaro reaction, in which the formaldehyde acts as a sacrificial reducing agent to reduce the formyl group of HMF, resulting in BHMF and sodium formate after more than 6 hours.[22] In the last method, reduction of HMF to BHMF is achieved through hydrogen transfer (hydrogenation), typically from H_2, as shown in Figure 1. Metal catalysts such as $2CuO{\cdot}Cr_2O_3$, Pt/C, PtO, and Ru/C under high pressures of H_2 (28-350) and elevated temperatures (403-423 K) have achieved up to 100% conversion of HMF to BHMF in as little as 30 minutes and as long as 12 hours.[23-26]

Hydrogenation and hydrogenolysis (addition of H_2 and loss of H_2O) of HMF (or hydrogenolysis of preformed BHMF) results in DMF. DMF, a water insoluble liquid, has an energy content similar to that of gasoline and 40% greater than ethanol (the current leading biofuel and gasoline additive), while also being less volatile than ethanol.[17] Current methods of HMF conversion to DMF commonly require high temperatures (393-573 K) and pressures of H_2

(6.8-62 bar) utilizing precious metal catalysts such as Pd, CuRu.[10,17,19] Recent work has been done to utilize other hydrogen sources, such as alcohols, resulting in the concurrent production of aldehydes and ketones.[27]

Reduction of HMF requires a significant amount of sacrificial reagents, or high temperatures and pressures of H_2. As H_2 is a valuable energy source that must be produced from other primary sources and alternative sources of hydrogen come from other valuable commodities, a new conversion method to utilize a cheaper, more sustainable and accessible source of hydrogen needs to be developed. Water is the cheapest and most abundant hydrogen source on earth. Therefore, developing a method to efficiently utilize hydrogen from water to reduce HMF could represent a major breakthrough toward moving away from a fossil fuel economy. Simple electrochemical processes allow for splitting water (simultaneous reduction and oxidation of water to H_2 and O_2) and may prove a viable pathway for reduction of HMF. The application of electrochemical methods to accomplish transformations of organic molecules (electrochemical organic synthesis, or electroorganic synthesis) is a promising and attractive approach since it provides a high degree of control over the selectivity of the reactions that occur.[28]

1.3. Electrochemical Organic Synthesis

In electrochemical organic synthesis, electrodes are immersed in a solvent containing an organic molecule (to be reduced at the cathode or oxidized at the anode) and a supporting electrolyte (dissolved ions to conduct the flow of charge between the cathode and anode in the solution).[28,29] The desired reaction, reduction or oxidation of the organic material, occurs at the working electrode. To sustain current (the flow of electrons through the circuit) an oxidation or reduction reaction, whichever is the opposite of the reaction at the working electrode, must occur

at the other electrode, defined as the counter electrode. By utilizing a third electrode of a known potential, called the reference potential, the potential applied to the working electrode, relative to the reference, can be controlled. In this manner a fine level of control over the selectivity of the organic oxidation or reduction reactions can be achieved.[28]

Because the electrodes are connected in a circuit, it is possible to measure the total charge, or number of electrons, that flow through the circuit and, consequently, are used in reduction and oxidation processes at the cathode and anode. Faradaic efficiency (FE) is a measure of efficiency for a reduction or oxidation reaction based on the total portion of electrons that flowed through the system that were used for the desired reaction. In order to prevent the oxidation of reduced species or *vice versa*, the cathode and anode are separated into two half cells separated by a porous glass frit or membrane that allows the flow of ions between the half cells but minimizes the crossover of the organic species.[29]

Utilizing electrochemistry for reduction of HMF and other biomass intermediates is an appealing alternative approach to the conventional methods discussed since it allows the use of H^+ or H_2O as the hydrogen source without the need of H_2 or other chemical reducing agents. Furthermore, it allows for a systematic study of the impact of applied potential, electrode material, pH, electrolyte, and number of other variables on the efficiency and selectivity of the organic transformations that take place.

1.4. Scope of Thesis Work

The work presented herein demonstrates newly developed electrochemical methods of converting biomass intermediates, with an eye to the future prospects of decreased petroleum dependence and greater utilization of biomass for our fuel, commodity chemical, and pharmaceutical needs.

In Chapter 2, the efficient electrochemical reduction of HMF to BHMF, an important monomer for industrial processes, is demonstrated using Ag catalytic electrodes. This process uses water as the hydrogen source at ambient conditions and eliminates the need to generate and consume H_2 for hydrogenation, providing a practical and efficient route for BHMF production. By systematic investigation of HMF reduction on the Ag electrode surface, BHMF production was achieved with the FE and selectivity nearing 100%, and plausible reduction mechanisms were also elucidated. Furthermore, construction of a photoelectrochemical cell (PEC) composed of an n-type $BiVO_4$ semiconductor anode, which uses photogenerated holes for water oxidation, and a catalytic Ag cathode, which uses photoexcited electrons from $BiVO_4$ for the reduction of HMF to BHMF, was demonstrated to utilize solar energy to significantly decrease the external voltage necessary for HMF reduction. This shows the possibility of coupling electrochemical HMF reduction and solar energy conversion, which can provide more efficient and environmentally benign routes for reductive biomass conversion.

In chapter 3, the direct electrochemical conversion of HMF to 2,5-hexanedione (HD) at ambient pressure and temperature is demonstrated without using H_2 or precious metal catalysts. Water was used as the hydrogen source and zinc was used as the catalytic electrode, which enabled hydrogenolysis and Clemmensen reduction coupled with furan ring opening. Optimum conditions to achieve high FE and selectivity for HD production were investigated and plausible mechanisms were proposed. The environmentally benign one-step procedure to produce HD reported in this study will serve as a new route to valorize biomass intermediates.

In chapter 4, the catalytic abilities and efficiencies of various metal electrodes (Ag, Cu, Pt, Sn, and Zn) were investigated for electrochemical reductive amination of HMF with methylamine (CH_3NH_2). For each metal electrode, potentials necessary to initiate reductive

amination as well as potential dependent FE and selectivity were investigated systematically. Based on the results, reduction conditions and a high surface area Ag electrode that can achieve a FE and a selectivity nearing 100% were reported. Furthermore, reductive amination of HMF derivatives such as 5-methylfurfural (5-MF), 2,5-diformylfuran (DFF), and 5-formyl-2-furancarboxylic acid (FFCA) using methylamine as well as reductive amination of HMF using ethanolamine ($HOCH_2CH_2NH_2$) were conducted to establish electrochemical reductive amination as a general route for reductive amination of furfural-based biomass intermediates.

In chapter 5, the recently developed method to cathodically deposit conductive polymer films is utilized for simultaneous deposition of metals and conductive polymers to yield high surface area metal-coated polymer films. The compositions and morphologies of the films are systematically altered by varying the concentrations of the metal ions in the deposition solution. The catalytic abilities of the films for electrochemical reduction of CO_2 are analyzed and compared to metal foil electrodes. Initial results demonstrate greater efficiencies with the metal-polymer films, though this remains an unfinished work.

1.5. References

1. G.W. Huber, S. Iborra, and A. Corma, *Chem. Rev.,* 2006, **106**, 4044-4098.
2. A. A. Rosatella, S. P. Simeonov, R. F. M. Frade and C. A. M. Alfonso, *Green Chem.,* 2011, **13**, 754-793.
3. D. T. Whipple and P. J. A. Kenis, J. *Phys. Chem. Lett.* 2010, **1**, 3451-3458.
4. R. –J. van Putten, J. C. van der Waal, E. de Jong, C. B. Rasrendra, H. J. Heeres and J. G. de Vries, *Chem. Rev.,* 2013, **113**, 1499-1597.
5. M. Mikkelsen, M. Jorgensen and F. C. Krebs, *Energy Environ. Sci.*, 2010, **3**, 43.
6. A. C. O'Sullivan, *Cellulose*, 1997, **4**, 173-207.
7. D. Klemm, B. Heublein, H. –P. Fink and A. Bohn, *Angew. Chem. Int. Ed.,* 2005, **44**, 3358-3393.
8. F. Fuo, Z. Fang, C. C. Xu and R. L. Smith Jr., *Prog. Energy Combust. Sci.*, 2012, **38**, 672-690.
9. A. Corma, S. Iborra and A. Velty, *Chem. Rev.*, 2007, **107**, 2411-2502.
10. J. B. Binder and R. T. Raines, *J. Am. Chem. Soc.*, 2009, **131**, 1979-1985.
11. W. –H. Peng, Y. –Y. Lee, C. Wu and K. C. –W. Wu, *J. Mater. Chem*., 2012, **22**, 23181-23185.
12. J. J. Bozell and G. R. Petersen, *Green Chem.*, 2010, **12**, 539-554.
13. J. Q. Bond, A. A. Upadhye, H. Olcay, G. A. Tompsett, J. Jae, R. Xing, D. M. Alonso, D. Wang, T. Zhang, R. Kumar, A. Foster, S. M. Sen, C. T. Maravelias, R. Malina, S. R. H. Barrett, R. Lobo, C. E. Wyman, J. A. Dumesic and G. W. Huber, *Energy Environ. Sci.*, 2014, **7**, 1500-1523.
14. G. W. Huber and J. A. Dumesic, *Catal. Today*, 2006, **111**, 119-132.

15. M. Balakrishnan, E. R. Sacia and A. T. Bell, *Green Chem.*, 2012, **14**, 1626-1634.

16. J. M. R. Gallo, D. M. Alonso, M. A. Mellmer and J. A. Dumesic, *Green Chem.*, 2013, **15**, 85-90.

17. Y. Roman-Leshkov, C. J. Barrett, Z. Y. Liu and J. A. Dumesic, *Nature*, 2007, **447**, 982-986.

18. E. Sacia, M. Deaner, Y. Louie and A. Bell, *Green Chem.*, 2015, **17**, 2393-2397.

19. M. Chidambaram and A. T. Bell *Green Chem.*, 2010, **12**, 1253-1262.

20. L. Cottier, G. Descotes and Y. Soro, *Synth. Commun.,* 2003, **33**, 4285-4295.

21. S. Goswami, S. Dey and S. Jana, *Tetrahedron,* 2008, **64**, 6358-6363.

22. J. H. Turner, P. A. Rebers, P.L. Barrick and R. H. Cotton, *Anal. Chem.,* 1954, **26**, 898.

23. V. Schiavo, G. Descotes and J. Mentech, *Bull. Soc. Chim. Fr.,* 1991, **128**, 704-711.

24. A. Faury, A. Gaset and J. P. Gorrichon, *Informations chimie,* 1981, **214**, 203-209.

25. R. Alamillo, M. Tucker, M. Chia, Y. Pagan-Torres and J. Dumesic, *Green Chem.,* 2012, **14**, 1413-1419.

26. J. Ohyama, A. Esaki, Y, Yamamoto, S. Arai and A. Satsuma, *RSC Adv.,* 2013, **3**, 1033-1036.

27. D. Scholz, C. Aellig and I. Hermans, *ChemSusChem*, 2014, **7**, 268-275.

28. E. Steckhan, in *Laboratory Techniques in Electroanalytical Chemistry,* ed. P. Kissinger, W. R. Heineman, Marcel Dekker, New York, 2nd edition, 1996, 22, 641-681.

29. J. Grimshaw, *Electrochemical Reactions and Mechanisms in Organic Chemistry*, Elsevier, Amsterdam, 2000.

Chapter 2. Efficient and Selective Electrochemical and Photoelectrochemical Reduction of 5-hydroxymethylfurfural to 2,5-bis(hydroxymethyl)furan Using Water as the Hydrogen Source

Portions of this chapter were published as:

J. J. Roylance, T. W. Kim and K. –S. Choi, *ACS Catal.*, 2016, **6**, 1840-1847.

2.1. Introduction

As discussed in chapter 1, biomass conversion can provide a viable pathway to minimize our dependence on petroleum products for generating both fuels and organic chemicals used in various industrial processes.[1-6] BHMF, which is produced by reduction of the formyl group of HMF, is an important starting molecule for various industrially important polymerization or etherification processes (e.g. biodiesel, polyester, and polyurethane foams).[2,7-9] To date, the conversion of HMF to BHMF has been mainly achieved by using H_2 as the hydrogen source in a pressurized cell (28-350 bar) operating at high temperatures (403-423 K) using various heterogeneous catalysts, usually containing precious metals (Figure 2.1a).[10-13] Considering that H_2 itself is a valuable energy source that must be produced from other primary sources with an energy input, enabling reductive biomass conversion without consuming H_2 would be highly beneficial.[14,15]

Recently, the possibility of electrochemically reducing HMF to BHMF (Figure 2.1b) and other reduced species utilizing H^+ or H_2O as the hydrogen source was demonstrated.[16-18] This process is very appealing because it does not consume H_2. However, in order to make electrochemical biomass conversion a practical and efficient alternative pathway for reductive biomass conversion, two major issues need to be addressed. First, since electrochemical HMF reduction in aqueous media always competes with water reduction to H_2, the FE for HMF reduction is expected to be low. Therefore, the development of catalytic electrodes and reduction conditions that can significantly increase FE as well as selectivity is critical. Previous studies did not report FE for the production of BHMF and the highest selectivity reported for BHMF production was 77%.[16-18] Second, since the electrochemical reduction of HMF requires electrical energy input, a strategy to minimize that input while achieving high FE and selectivity

is essential. Any conditions and strategies that can address these issues will be advantageous not only for HMF reduction but also for the reduction of related biomass intermediates like furfurals.

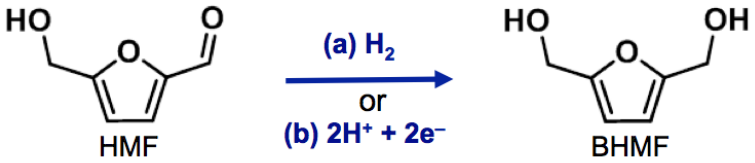

Figure 2.1. Conversion of HMF to BHMF (a) by conventional hydrogenation using H_2 as the hydrogen source and (b) by electrochemical hydrogenation using H^+ from H_2O as the hydrogen source.

This study reports the electrochemical reduction conditions using catalytic Ag cathodes that can convert HMF to BHMF using H_2O as the hydrogen source with FE and selectivity nearing 100% at ambient pressure and temperature. Also demonstrated is the construction of a photoelectrochemical cell (PEC) by simply replacing a dark anode with an n-type $BiVO_4$ semiconductor electrode (photoanode) that can directly utilize solar energy for HMF reduction, significantly decreasing the external energy input necessary for reduction. Previously, for cleaner and more sustainable biomass conversion, it was envisioned that the H_2 gas required for reductive biomass conversion would be provided from H_2 produced by renewable sources such as solar water splitting.[1,19] The PEC presented in this study demonstrates the possibility of directly utilizing solar energy and water for HMF reduction without involving the formation and use of H_2.

2.2. Experimental

2.2.1. Materials

Copper foil was purchased from Nimrod Hall Copper Foil Company. Boric acid (≥ 98.5%), sodium hydroxide (≥ 97%), and 5-hydroxymethylfurfural (≥ 99%) were purchased from Sigma Aldrich. Silver nitrate (99.9+%) was purchased from Alfa Aesar. To assist in method development, standard calibration, and product identification, 2,5-bis(hydroxymethyl)furan (97%) was purchased from Polysciences, Inc. All chemicals were used without further purification.

2.2.2. Preparation of Electrodes

Cu electrodes used in this study were prepared by cutting Cu foil to pieces with a dimension of 1.5 cm x 2.5 cm. Cu tape was attached to the top of the Cu foil electrode to enable connection to the potentiostat lead. The backside and top 0.5 cm of the Cu foil were then covered with Teflon tape to yield a 3.0 cm^2 working area. High surface area Ag electrodes (hereafter referred to as Ag_{gd}) were prepared by galvanic displacement, which involved immersing clean Cu-foil electrodes (1.5 cm x 2.0 cm working area) into a 50.0 mM solution of $AgNO_3$ for 30 seconds. The concentration of the Ag^+ solution and the duration of deposition reported here are optimum conditions to produce uniform and adherent Ag electrodes. Increasing the Ag^+ concentration, which increased the deposition rate of Ag, resulted in poor adhesion of Ag on the Cu surface. Decreasing the Ag^+ concentration resulted in nonuniform coverage of Ag on the Cu surface. In a similar manner, increasing or decreasing the deposition time affected the adhesion or uniformity of the Ag deposition. To achieve good coverage and adhesion of Ag on the Cu, the Cu foil electrodes were cleaned just prior to deposition by rinsing with 2-propanol and water followed by immersing in 1 M HCl for 1 minute to remove surface

oxides. They were then rinsed with water, dried, and immediately placed in the $AgNO_3$ solution. Following deposition, the film was rinsed gently with water and dried in an air stream.

Morphologically flat Ag electrodes (hereafter referred to as Ag_{sp}) were prepared by sputter coating. To prepare Ag_{sp} electrodes, Cu foil cleaned using aforementioned procedures was placed in a sputter coater (Anatech USA, DC/RF Dual Source Sputtering System) where 100 nm of Ag was sputter-coated onto the Cu substrate. The films were then made into electrodes in the same manner as for the Cu-foil electrodes. The Pt counter electrodes were prepared by sputter coating a 100 nm platinum layer over a 20 nm titanium layer onto cleaned glass slides. The dimension of the working area of the Pt counter electrode was 2.0 cm x 2.0 cm. The nanoporous $BiVO_4$ electrode coated with oxygen evolution catalysts (FeOOH and NiOOH) used in the construction of a PEC was prepared using the procedures reported in a recent paper.[20]

2.2.3. Characterization

Ag_{gd} and Ag_{sp} electrodes were characterized by powder X-ray diffraction (XRD) (Bruker D8 Advanced PXRD, 298 K, Ni-filtered Cu K_α-radiation, λ = 1.5418 Å). Aside from the underlying copper substrate, only crystalline Ag peaks were observed for both films (Figure 2.2a). No other crystalline impurity peaks (e.g. Ag_2O, AgO) were detected.

When XRD patterns of the electrodes were obtained again after passing 20 C for HMF reduction at −1.3 V vs. Ag/AgCl, no change was observed (Figure 2.2b). The surface morphologies of the Ag_{gd} and Ag_{sp} electrodes were examined by Scanning Electron Microscopy (SEM) using a LEO 1530 microscope at an accelerating voltage of 5 kV before and after electrochemical HMF reduction at −1.3 V vs. Ag/AgCl. Again, no change was observed (Figure 2.3).

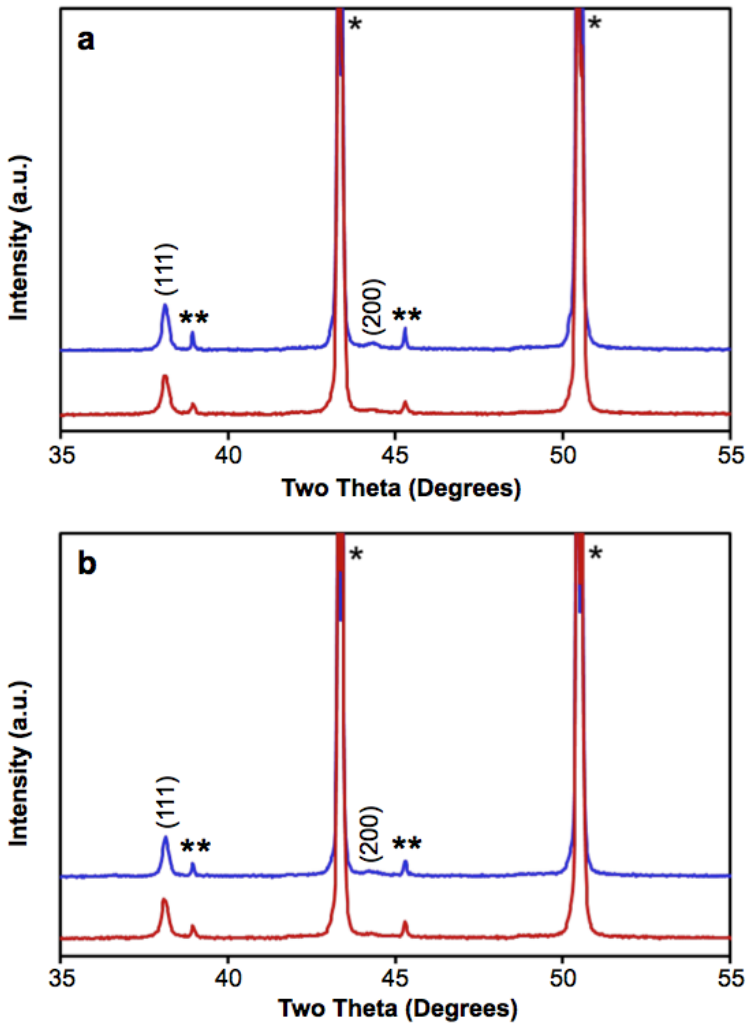

Figure 2.2. XRD patterns of Ag_{gd} (red) and Ag_{sp} (blue) electrodes (**a**) as-deposited and (**b**) after passing 20 C at −1.3 V vs. Ag/AgCl for HMF reduction. No changes are observed in the peak shape and height. The peaks from Cu foil are denoted by * and **. The peaks denoted by ** are Cu peaks generated by Cu K_β radiation, which could not be completely removed by the Ni filter. (When slow scanning conditions were used to collect Ag peaks from thin Ag electrodes, the intensities of the Cu peaks from strongly diffracting Cu foil generated by Cu K_β radiation were too strong to be completely removed by the Ni filter.)

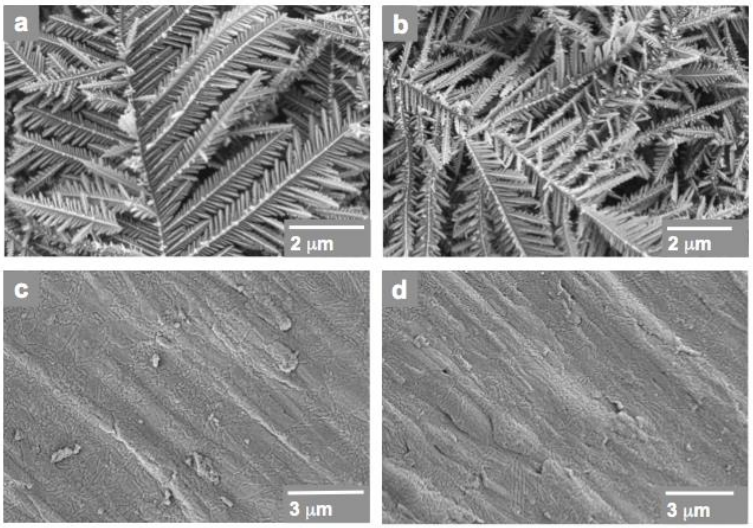

Figure 2.3. SEM images of Ag_{gd} electrodes (a) as-deposited and (b) after passing 20 C at −1.3 V vs. Ag/AgCl for HMF reduction. SEM images of Ag_{sp} electrodes (c) as-deposited and (d) after passing 20 C at −1.3 V vs. Ag/AgCl for HMF reduction.

2.2.4. Electrochemical HMF Reduction

To investigate the catalytic abilities of Cu foil, Ag_{gd}, and Ag_{sp} electrodes to reduce HMF, linear sweep voltammetry (LSV) was performed using solutions with and without HMF. The general experimental setup consisted of a three-electrode system (Cu or Ag working electrode, Pt counter electrode, and a Ag/AgCl (4 M KCl) reference electrode) in an undivided cell controlled by a Bio-Logic VMP2 potentiostat. A 0.5 M borate buffer solution (pH 9.2) with and without 0.02 M HMF was used as the electrolyte, which was purged with N_2 to remove dissolved oxygen prior to obtaining LSVs. The potential was swept to the negative direction from the open circuit potential to −1.5 V vs. Ag/AgCl (4 M KCl) at 5 mV/s without stirring. The results were plotted against both Ag/AgCl and the reversible hydrogen electrode (RHE). The latter allows easy interpretation of the data against the thermodynamic water reduction potential to H_2 in the pH

condition used in this study. All current densities reported in this study were calculated based on the geometric area of the working electrode.

Constant potential electrolysis experiments were conducted to quantify products, selectivities, and FE. A three-electrode setup was employed using an H-shaped cell divided by a glass frit. The Cu or Ag working electrode and the reference electrode were immersed in the cathodic compartment containing 14 mL of a 0.5 M borate buffer solution (pH 9.2) with 0.02 M HMF. The counter electrode was immersed in the anodic compartment containing 14 mL of a 0.5 M borate buffer solution (pH 9.2) with 1 M sodium sulfite. Because sulfite oxidation occurs at a less positive potential than water oxidation, using sulfite oxidation as the counter electrode reaction prevented the drift of the anode potential to the potential limit of the potentiostat, which occasionally occurred when water oxidation was used as the counter electrode reaction because the divided cell used in this study was not optimized and caused a significant IR drop during electrolysis. For a three-electrode setup, the counter electrode reaction does not affect the current generated at the working electrode. Therefore, using sulfite oxidation as the counter electrode reaction allowed us to prevent experimental issues unrelated to HMF reduction without affecting the results obtained at the working electrode.

Just prior to use in electrolysis, the working electrode was reduced in a separate borate buffer solution by performing a potential sweep from open circuit potential to −1.5 V vs. Ag/AgCl at 5 mV/s to ensure reduction of any surface oxide species so as to minimize Faradaic loss during HMF reduction. The designated potential was applied to the working electrode by a Bio-Logic VMP2 potentiostat for a duration of 20 C, after which time the solution was collected and analyzed. Mass transport of the HMF solution during the electrolysis was facilitated by magnetic stirrer at approximately 1600 rpm.

2.2.5. Product Analysis

Products were detected and quantified using a Bruker Avance III 400 MHz nuclear magnetic resonance (NMR) spectrometer. Calibration curves were generated for both BHMF and HMF by obtaining NMR spectra for a series of solutions of known concentration for each species and plotting the area obtained for signature HMF and BHMF peaks for each concentration. The area for HMF and BHMF peaks of unknown concentrations from the product solution were then plotted against the calibration curves to determine their concentrations. The HMF peaks in the product solution were also compared to those of the initial solution to determine the amount of HMF consumed. Since the samples were aqueous solutions, the NMR spectra were collected and processed using a water suppression method to remove the ^{1}H signal from water. As a result, signals for peaks near water (4.7 ppm) were significantly decreased. Water suppression did not affect quantifications of HMF and BHMF.

2.2.6. Photoelectrochemical HMF Reduction

LSVs for photoelectrochemical HMF reduction were performed in an undivided cell without stirring using the same solution and procedures described above. The only difference was that the Pt anode was replaced by a $BiVO_4$ photoanode, and the reference electrode was removed to form a two-electrode system.

Illumination of the $BiVO_4$ photoanode was achieved through the FTO substrate (back-side illumination) with an Oriel LCS-100 solar simulator with the intensity of the incident light calibrated to be AM1.5G, 100 mW/cm^2. The result was compared with LSVs obtained using a two-electrode system composed of a Ag_{gd} working electrode and a Pt counter electrode. For this comparison, the sizes of all working and counter electrodes were kept as 1 cm^2.

Constant potential electrolysis was performed by applying 1.0 V between the Ag_{gd} cathode and the $BiVO_4$ photoanode (a two-electrode cell) and passing 5 C under illumination (AM 1.5G, 100 mW/cm^2) using a divided cell. A 0.5 M borate buffer solution (pH 9.2) was used as the electrolyte and the solution in the cathodic compartment contained 0.02 M HMF. This time sulfite was not added to the anodic compartment because the potential necessary for full cell operation with the presence of only HMF and water as electrochemically active species needed to be evaluated accurately. The cell reactions are summarized in the section 2.3.

When a two-electrode cell is used, while the potential difference between the cathode and the anode is fixed at 1.0 V, the absolute potentials applied to the working electrode and the counter electrode are not fixed and can be influenced by various conditions. As discussed below, the results of a three-electrode potential-dependence study showed that –1.3 V vs. Ag/AgCl (equivalent to –0.56 V vs. RHE) is an optimum potential for the Ag_{gd} electrode to reduce HMF to BHMF with the highest selectivity and FE. Therefore, while 1.0 V was applied between the working electrode and the counter electrode, other conditions were optimized to ensure that the potential applied to the Ag_{gd} electrode is near –1.3 V vs. Ag/AgCl by monitoring the potential between the Ag_{gd} and a Ag/AgCl (4M KCl) reference electrode, which was not connected to a potentiostat, using a multimeter. This included making the size of the $BiVO_4$ (2 cm^2) 4 times larger than the size of the Ag_{gd} electrode (0.5 cm^2) and stirring only in the $BiVO_4$ anode compartment. The latter condition facilitated the current generation at the anode, which in turn resulted in the application of a more negative potential to the Ag_{gd} cathode to generate a matching current. As a result, a desired potential, ~ –1.3 V vs. Ag/AgCl, was achieved at the Ag_{gd} electrode during the constant potential electrolysis at 1.0 V between the Ag_{gd} cathode and

the $BiVO_4$ photoanode, which resulted in the production of BHMF with a FE of 94% and a selectivity of 95%.

2.3. Results and Discussion

When HMF is reduced in an aqueous solution, water reduction to H_2 is the major competing reaction. Therefore, identifying good HMF reduction catalysts among poor H_2 evolution catalysts can be a good strategy for minimizing a FE loss due to water reduction. This is one of the major reasons why lead, mercury, and cadmium electrodes were often used for electroorganic synthesis in aqueous media.[14,15,21-23] In this study silver and copper electrodes, which are also known to be poor H_2 evolution catalysts while not being toxic,[24] were investigated for HMF reduction. High surface area Ag cathodes, which were discovered to be particularly catalytic for BHMF formation in this study, were prepared by galvanically displacing a piece of commercially available Cu foil with Ag in a 0.05 M $AgNO_3$ solution for 30 s (referred to as Ag_{gd} in this study). The displacement reaction was kinetically fast and quickly depleted Ag^+ ions at the Cu surface. As a result, the growth of Ag was limited by diffusion of Ag^+ ions, and Ag electrodes with a dendritic fractal morphology were obtained (Figure 2.4a).[25,26] This morphology is favorable for increasing surface area while maintaining good electrical continuity between Ag crystals.[26]

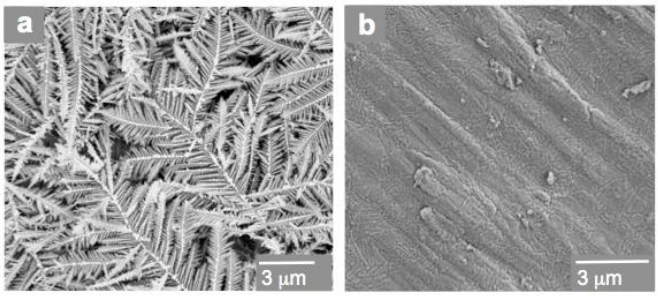

Figure 2.4. SEM images showing the surface morphologies of (a) Ag_{gd} and (b) Ag_{sp} electrodes.

2.3.1. Linear Sweep Voltammetry

The catalytic ability of the Ag_{gd} electrode for HMF reduction as the half-cell reaction was first investigated by linear sweep voltammetry (LSV) with and without 0.02 M HMF. The LSVs were measured in an undivided three-electrode cell containing a 0.5 M borate buffer solution (pH 9.2). The LSVs of the Cu foil used as the substrate for preparing Ag electrodes and a morphologically flat Ag electrode prepared by sputter coating Ag onto Cu foil (Figure 2.4b), referred to as $Ag_{sp,}$ are also shown for comparison. Since the effective surface area of the Ag_{gd} electrode is unknown, current density has been normalized to the geometric area of the electrodes, 3 cm^2.

The cathodic currents observed in the solution without HMF are due to the reduction of water to H_2 (Figure 2.5a). When 0.02 M HMF was added to the solution, all electrodes showed a shift of the cathodic current onset potential to the positive direction (Figure 2.5b). This indicates that HMF reduction is easier than water reduction on the Ag and Cu electrodes. For the case of both the Ag_{gd} and Ag_{sp} electrodes, a distinctive cathodic wave for HMF reduction could be observed. In particular, the Ag_{gd} electrode showed the most significant changes in onset potential shift and current density for HMF reduction. Figure 2.5a shows that the onset potentials of the Ag_{gd} and Ag_{sp} electrodes for water reduction are comparable to each other, although the current of the Ag_{gd} electrode after the onset increases more rapidly due to its higher surface area. However, for the case of HMF reduction (Figure 2.5b), the Ag_{gd} electrode shows a distinctively more positive onset potential compared with the Ag_{sp} electrode, indicating that the Ag_{gd} electrode is particularly more catalytic for HMF reduction. The Ag_{gd} electrode, which is composed of dendritic nanocrystals, likely offers effective binding sites for HMF molecules that can facilitate interfacial charge transfer processes for HMF reduction. The potentials required to

generate 1 mA/cm^2 of current density when HMF was present were –0.33 V, –0.44 V, and –0.48 V vs. RHE, respectively, for Ag_{gd}, Ag_{sp}, and Cu foil electrodes. It should be noted that the reduction of HMF to BHMF is not reversible on these electrodes judging from the cyclic voltammograms (CVs) obtained using the same conditions (Figure 2.6).

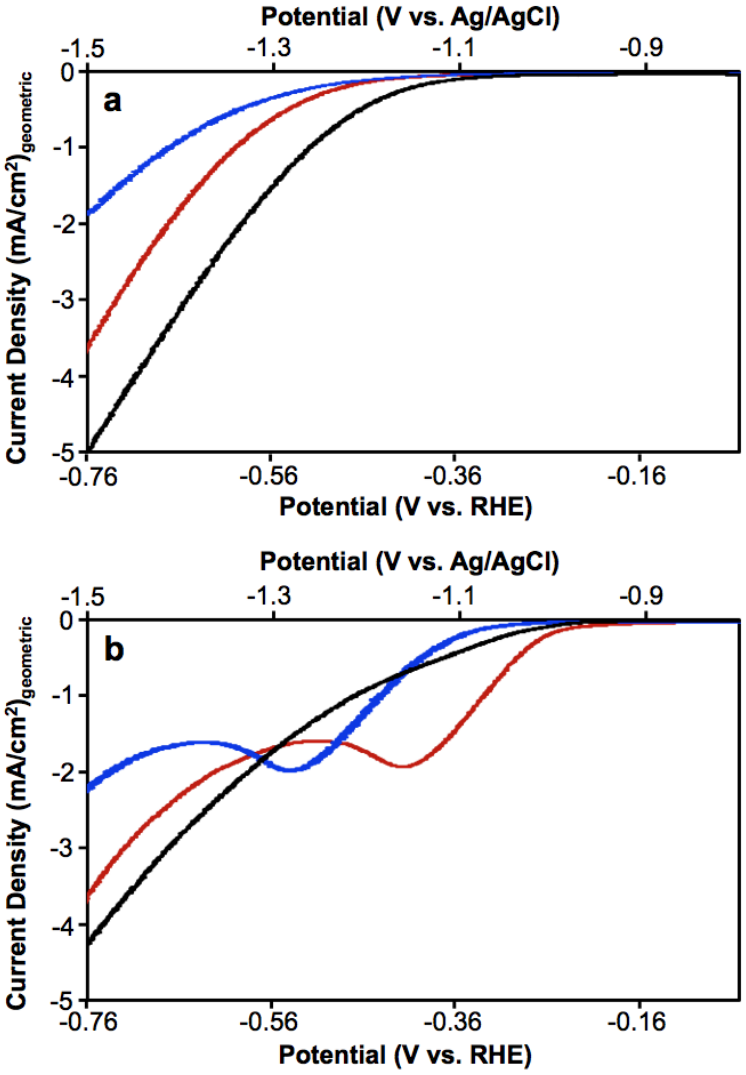

Figure 2.5. LSVs of Cu (black), Ag_{sp} (blue), and Ag_{gd} (red) electrodes in 0.5 M borate buffer (pH 9.2) (a) without and (b) with 0.02 M HMF (scan rate: 5 mV/s).

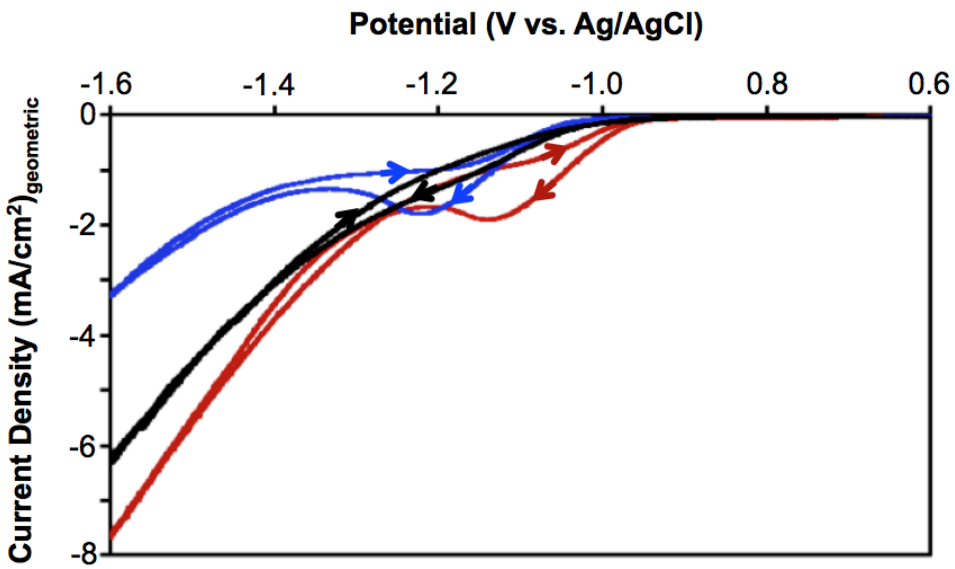

Figure 2.6. CVs of Cu (black), Ag_{sp} (blue), and Ag_{gd} (red) electrodes in 0.5 M borate buffer (pH 9.2) with 0.02 M HMF (scan rate: 5 mV/s). The current profiles on the reverse scan show that the reduction of HMF to BHMF is not reversible on these electrodes under the given conditions.

2.3.2. Constant Potential Electrolysis

The reduction products and conversion efficiencies for HMF reduction were analyzed by performing HMF reduction in a divided cell at a constant potential of −1.3 V vs. Ag/AgCl (equivalent to −0.56 V vs. RHE) by passing 20 C in 14 mL of 0.5 M borate buffer solution containing 0.02 M HMF. After reduction, the electrolyte was analyzed by ^{1}H-NMR to quantify the amounts of BHMF and remaining HMF (Figure 2.7). Based on these results, FE and selectivity for BHMF formation, which are summarized in Table 2.1, were calculated using equations 2.1 and 2.2, where F is the Faraday constant (96485 C/mol).

$$\text{FE}\ (\%) = \frac{\text{mol of BHMF formed}}{\text{Total charge passed (C)} \,/\, (\text{F}\times 2)} \times 100\% \qquad (2.1)$$

$$\text{Selectivity of BHMF}\ (\%) = \frac{\text{mol of BHMF formed}}{\text{mol of HMF consumed}} \times 100\% \qquad (2.2)$$

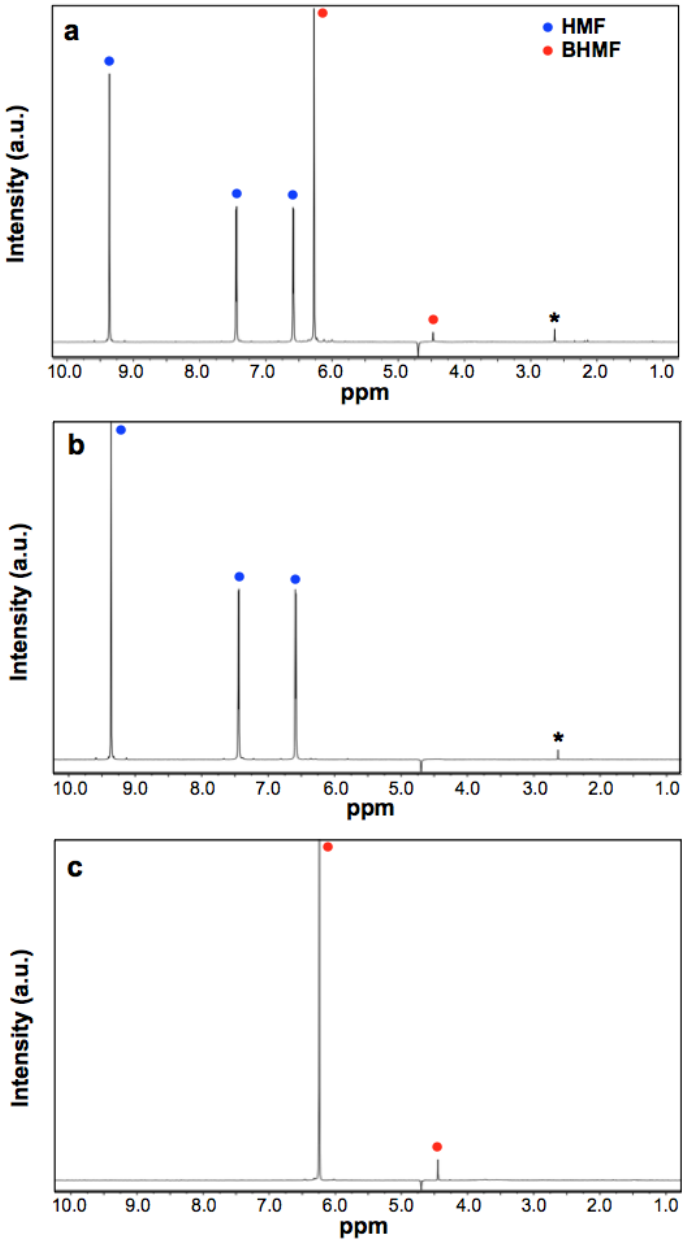

Figure 2.7. ^{1}H-NMR spectra for (a) an HMF solution after passing 20 C at –1.3 V vs. Ag/AgCl to the Ag_{gd} electrode for HMF reduction, (b) a fresh HMF solution, and (c) a fresh BHMF solution: ^{1}H NMR (400 MHz, 90% H_2O/ 10% D_2O) δ 9.36 (s, 1H), 7.45 (d, J = 3.9 Hz, 1H), 6.59 (d, J = 3.9 Hz, 1H), 6.24 (s, 2H), 4.45 (s, 4H). HMF peaks at 9.36, 7.45, and 6.59 ppm. BHMF peaks at 6.24 and 4.45 ppm. The BHMF peak at 4.45 ppm is diminished by water suppression. The peak marked with * is from a dimethylsulfoxide impurity present in the as-purchased HMF.

Table 2.1. Results obtained from electrochemical reduction of HMF to BHMF by Ag_{gd}, Ag_{sp}, and Cu electrodes.[a] Average values obtained from three measurements are shown. For FE and selectivity, standard deviations are shown in parentheses.

Electrode	Average current density (mA/cm^2)	HMF consumed (mmol)	BHMF formed (mmol)	Rate for BHMF production ($mmol/h/cm^2$)	FE (%)	Selectivity (%)
Ag_{gd}	6.90	0.104	0.102	0.127	99(2)	99(3)
Ag_{sp}	2.53	0.089	0.75	0.034	72(1)	84(7)
Cu	1.32	0.053	0.020	0.0047	19(1)	39(9)

[a] Reaction conditions: E = –1.3 V vs. Ag/AgCl (= –0.56 V vs. RHE) in a 0.5 M borate buffer (pH 9.2) containing 0.02 M HMF for 20 C passed.

The FE and selectivity for BHMF formation by the Ag_{gd} electrode were, remarkably, both 99%. This means that formation of H_2 and other HMF reduction products is negligible. The FE and selectivity for BHMF formation were 72% and 84%, respectively, for the Ag_{sp} electrode and 19% and 39%, respectively, for the Cu foil electrode. The decrease in selectivity was due to the formation of C-C bonds between HMF molecules, forming dimeric and polymeric species based on the NMR data.[27] No other reduction products were detected. The FEs of the Ag_{sp} and Cu foil electrodes, which are much lower than their selectivities for BHMF formation, indicate that part of the cathodic current was used for H_2 production.

After the reduction process, the composition, crystallinity, and morphology of the Ag_{gd} electrode were reexamined by SEM and XRD. No sign of instability or deformation of the Ag surface or composition was observed (Figures 2.2 and 2.3). When the same Ag_{gd} electrode was used for multiple HMF reduction experiments, starting with a fresh HMF solution every time, similar current density-time (*j*-*t*) plots were obtained (Figure 2.8), also confirming the stability of the Ag_{gd} electrode.

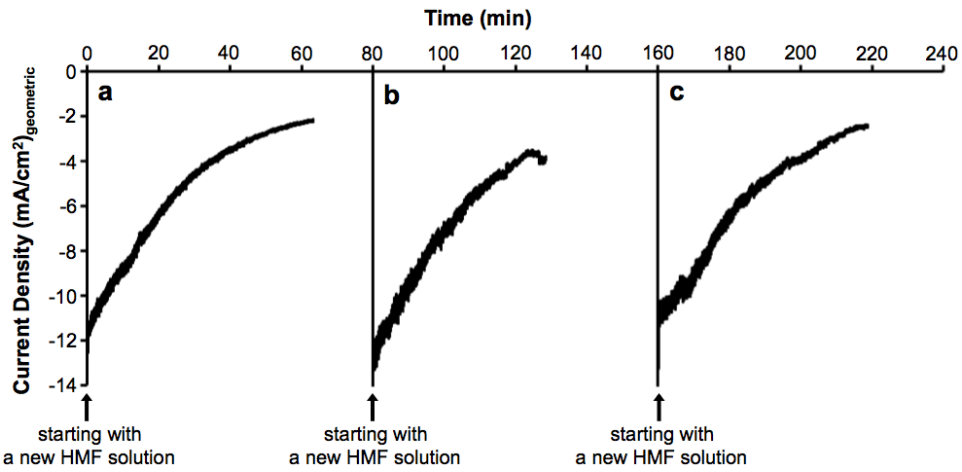

Figure 2.8. *J-t* plots obtained for three consecutive HMF reduction experiments labeled as (a), (b), and (c) using the same Ag_{gd} electrode. For each trial, a freshly prepared 0.02 M HMF solution in 0.5 M borate buffer (pH 9.2) was used and 60 C was passed for the complete conversion of HMF to BHMF. The slight difference in current density and time required to pass 60 C among these trials is due to the slight difference in the electrode locations in the cell.

Electrochemical HMF reduction using the Ag_{gd} electrode at various applied potentials was also performed, which can provide mechanistic insights for potential-dependent HMF reduction. The results are summarized in Table 2.2. Based on the FEs and selectivities of BHMF, the reduction potential could be divided into three regions. The first region is $-1.0\ V \geq E > -1.1\ V$ vs. Ag/AgCl. In this region, the amount of BHMF formed was much less than the amount of HMF consumed, meaning that there is a competing reaction consuming HMF, which lowers both the FE and selectivity for BHMF formation. The major competing reaction was the reaction between HMF molecules, which is the same competing reaction observed for the Cu and Ag_{sp} electrodes at −1.3 V vs. Ag/AgCl discussed above. The LSVs obtained without HMF (Figure 3a) show that H_2 evolution on the Ag_{gd} electrode initiates at −1.1 V vs. Ag/AgCl. Therefore, in this potential region, the reduction mechanism of HMF most likely does not

involve the formation of surface adsorbed hydrogen atoms (H_{ads}), which is the first step for H_2 evolution.[28] Then, HMF reduction proceeds either through e^- transfer to an HMF molecule to form an anionic intermediate that further reacts with H^+ or through simultaneous e^- transfer and H^+ transfer to HMF. Plausible mechanisms describing these pathways are shown in Figure 4 with blue arrows. In this case, the surface of the Ag_{gd} electrode is expected to be covered only with HMF or its reduction intermediates. As a result, reactions that form C-C bonds between HMF molecules and/or their reduction intermediates can be possible competing reactions in this potential region.

Table 2.2. Results obtained from electrochemical reduction of HMF to BHMF by a Ag_{gd} electrode.[a] Average values obtained from three measurements are shown. For FE and selectivity, standard deviations are shown in parentheses.

Potential (V vs. Ag/AgCl)	Average current density (mA/cm^2)	HMF consumed (mmol)	BHMF formed (mmol)	Rate for BHMF production ($mmol/h/cm^2$)	FE (%)	Selectivity (%)
−1.0	0.460	0.059	0.028	0.0023	27(3)	48(5)
−1.05	1.14	0.097	0.065	0.013	63(5)	68(8)
−1.1	2.47	0.101	0.082	0.036	79(2)	81(2)
−1.2	3.21	0.101	0.091	0.052	87(4)	89(7)
−1.3	6.90	0.104	0.102	0.127	99(2)	99(3)
−1.4	7.06	0.102	0.101	0.128	97(2)	99(3)
−1.5	7.97	0.100	0.099	0.14	96(2)	98(3)
−1.6	10.2	0.096	0.094	0.17	90(3)	97(7)
−1.7	12.0	0.088	0.086	0.19	87(7)	98(4)
−1.8	18.0	0.059	0.058	0.19	56(7)	98(2)

[a] Reaction conditions: $-1.0\ V \geq E \geq -1.8\ V$ vs. Ag/AgCl in a 0.5 M borate buffer (pH 9.2) containing 0.02 M HMF for 20 C passed.

The second potential region is $-1.1\ V \geq E > -1.6\ V$ vs. Ag/AgCl where both the FE and selectivity for BHMF formation increase considerably and become near 100%. This suggests that the reactions between HMF molecules considerably diminish in this potential region. LSVs obtained without HMF (Figure 3a) indicate that H_2 evolution and, therefore, the formation of H_{ads} are possible on the Ag_{gd} electrode surface in this region. This means new mechanisms that involve the formation of H_{ads} for BHMF production are possible in this potential region, which are indicated with red arrows in Figure 4. As the coverage of H_{ads} increases on the electrode surface and the rate of BHMF formation increases, the probability of HMF molecules adsorbing in close enough proximity on the electrode surface decreases, and the HMF-HMF reactions can be effectively suppressed.

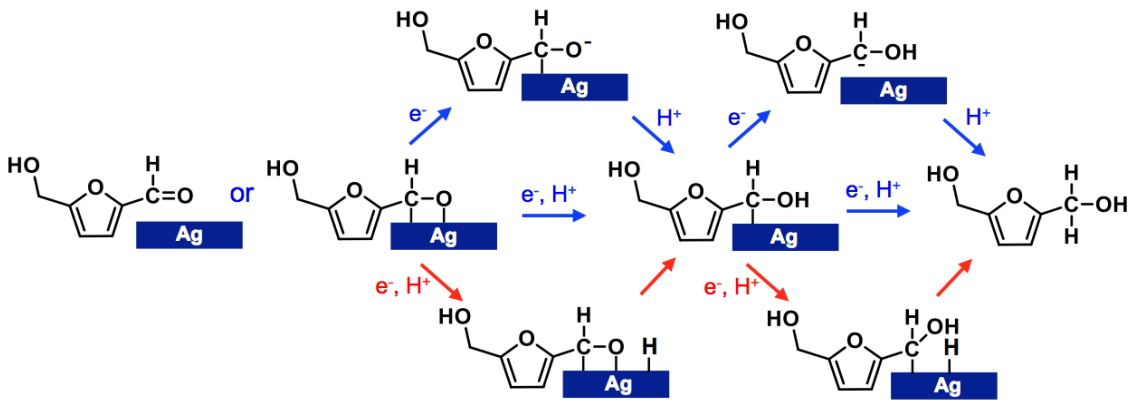

Figure 2.9. Plausible HMF hydrogenation mechanisms. Blue arrows represent hydrogenation pathways that do not involve the formation of adsorbed H atom (H_{ads}). Red arrows indicate additional pathways available when the formation of H_{ads} is enabled.

The third potential region is $E \leq -1.6$ V vs. Ag/AgCl, where H_2 evolution competes with BHMF formation, lowering the FE for BHMF formation. However, since there is no competing reaction consuming HMF in this region, the amount of HMF consumed is lowered accordingly. As a result, the selectivity for BHMF remains high in this region. In addition, since the current density in this high overpotential region is significantly increased, the conversion rates for BHMF are higher than those in the low overpotential regions (Table 2.2).

The change in FE and selectivity during electrochemical reduction using 0.02 M and 0.10 M HMF solutions buffered with borate (pH 9.2) was also monitored to examine the effect of HMF concentration on the FE and selectivity (Tables 2.3 and 2.4). For the case of 0.02 M solution, the FE and selectivity remained above 89% and 99%, respectively, during the complete conversion of HMF to BHMF. For the case of 0.10 M HMF solution, both the FE and selectivity were lower than those obtained for the 0.02 M HMF solution because the higher concentration of HMF resulted in enhanced adsorption of HMF on the Ag surface, which facilitated the undesired dimerization and polymerization reactions of HMF molecules.

Table 2.3. Changes in FE and selectivity for BHMF production during electrochemical HMF reduction by a Ag_{gd} electrode at -1.3V vs Ag/AgCl in a 0.5 M borate buffer (pH 9.2) containing 0.02 M HMF after every 10 C passed.

Charge passed (C)	Average current density (mA/cm^2)	HMF consumed (μmol)	BHMF formed (μmol)	Rate for BHMF production ($\mu mol/h/cm^2$)	FE (%)	Selectivity (%)
10	9.20	51.6	49.6	164	96	96
20	6.90	104	102	127	99	99
30	5.55	155	154	103	99	> 99
40	5.73	206	204	105	98	> 99
50	4.86	238	237	83.0	92	> 99
60	5.27	279	278	87.7	89	> 99

Table 2.4. Changes in FE and selectivity for BHMF production during electrochemical HMF reduction by a Ag_{gd} electrode at -1.3 V vs Ag/AgCl in a 0.5 M borate buffer (pH 9.2) containing 0.10 M HMF after every 50 C passed.

Charge passed (C)	Average current density (mA/cm^2)	HMF consumed (μmol)	BHMF formed (μmol)	Rate for BHMF production ($\mu mol/h/cm^2$)	FE (%)	Selectivity (%)
50	9.54	426	203	139	78	48
100	8.98	697	418	135	81	60
150	7.72	931	627	116	81	68
200	5.90	1.07×10^3	813	86.3	80	76

After evaluating the Ag_{gd} electrode as an optimum catalytic cathode for HMF reduction, a PEC was constructed to demonstrate how simply replacing a metal anode in an electrochemical cell with a semiconductor anode (photoanode) can significantly decrease the external energy input necessary for HMF reduction (Figure 2.10a) by utilizing solar energy. For the purpose of demonstrating this concept, n-type $BiVO_4$ was chosen as the photoanode, which has been recently identified as one of the most efficient and practical oxide-based photoanodes for use in solar water splitting.[20,29] As discussed below, it has favorable conduction band and valence band edge positions suitable to utilize photogenerated charge carriers for HMF reduction and water oxidation while being stable at pH 9.2 used for HMF reduction in this study.

Under illumination, electron-hole pairs were generated and separated in $BiVO_4$. The holes were used at the $BiVO_4$ surface to oxidize water to O_2, while the photoexcited electrons in the conduction band (CB) of $BiVO_4$ were transferred to the Ag cathode to reduce HMF to BHMF (Figure 2.10a). Because the bare surface of $BiVO_4$ is poorly catalytic for water oxidation, the surface of the $BiVO_4$ electrode was coated with layers of oxygen evolution catalysts (OECs) (i.e. FeOOH and NiOOH) to facilitate water oxidation to O_2.[20] The cell reactions are summarized in equations (2.3-2.5). The standard free energy change ($\Delta G°$) of the overall reaction (equation 2.5) at 298 K is calculated to be 211.20 kJ/mol,[30] which is thermodynamically more favorable than water splitting ($\Delta G° = 237.14$ kJ/mol). This means that direct electrochemical reduction of HMF using water as the hydrogen source is more energy efficient than the two-step procedure composed of water reduction to H_2, followed by the use of H_2 for hydrogenation.

$$\text{Cathode Reaction: HMF} + 2H^+ + 2e^- \rightarrow \text{BHMF} \qquad (2.3)$$

$$\text{Anode Reaction: } H_2O \rightarrow 1/2O_2 + 2H^+ + 2e^- \qquad (2.4)$$

$$\text{Overall: HMF} + H_2O \rightarrow \text{BHMF} + 1/2O_2 \qquad (2.5)$$

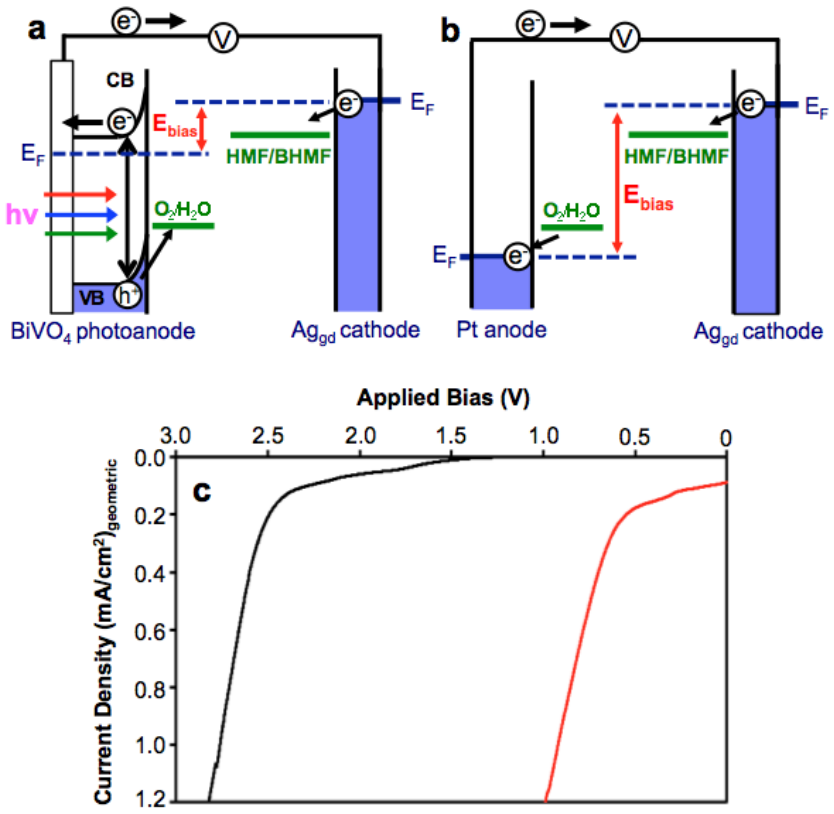

Figure 5. Schematic diagrams comparing the external bias necessary to achieve HMF reduction for (a) photoelectrochemical cell and (b) electrochemical cell. (c) LSVs obtained from photoelectrochemical cell (red) and electrochemical cell (black) for HMF reduction using a two-electrode cell (scan rate: 5 mV/s, illumination for photoelectrochemical cell: AM 1.5G, 100 mW/cm^2). A 0.5 M borate buffer solution (pH 9.2) containing 0.02 M HMF was used as the electrolyte.

Since the photoexcited electrons in the CB of $BiVO_4$ already possess a significantly negative potential (~ 0.0 vs. RHE),[20] the additional potential necessary to reduce HMF to BHMF can be decreased considerably (Figure 2.10a). Also, since the valence band (VB) edge of $BiVO_4$ is located at ~2.4 V vs. RHE, the photogenerated holes in the VB of $BiVO_4$ have sufficient overpotential for water oxidation before applying any external bias, which decreases the external bias necessary for the cell operation. This is quite different from the case of an electrochemical

cell where sufficient overpotentials for both the cathode reaction (HMF reduction) and for the anode reaction (water oxidation) need to be provided by the external bias (Figure 5b).

The advantage of using solar energy in decreasing external bias to reduce HMF is well demonstrated in Figure 2.10c comparing an LSV obtained from a two-electrode cell composed of a Ag_{gd} cathode and a Pt anode with that obtained from a PEC composed of a Ag_{gd} cathode and a $BiVO_4$/OEC photoanode under AM 1.5G illumination. For this experiment, the use of a two-electrode system was critical because the goal was to evaluate the electrical energy input (i.e. applied bias between the working and the counter electrode) necessary for HMF reduction. LSVs obtained using a three electrode cell show the change in current density when the potential between the working electrode and the reference electrode is varied, as shown in Figure 2.5. Experiments using a three-electrode cell are important for analyzing the half-cell reaction occurring at the working electrode at a precisely controlled potential against the reference electrode. However, these measurements do not provide any information on the potential applied between the working electrode and the counter electrode and, therefore, cannot be used for evaluating the decrease in external energy input owing to the utilization of solar energy.

The electrolyte was a 0.5 M borate buffer solution (pH 9.2) containing 0.02 M HMF. In order to achieve a current density of 1 mA/cm^2 in an electrochemical cell, application of 2.76 V between the Ag_{gd} cathode and the Pt anode was necessary. However, when a PEC is used, 1 mA/cm^2 was achieved at a potential of 0.92 V between the Ag_{gd} cathode and the $BiVO_4$/OEC anode, saving about 2 V. Results of a two electrode cell where a $BiVO_4$/OEC electrode was used as the anode both for an electrochemical cell in the dark and for a photoelectrochemical cell (e.g. LSV comparisons with and without HMF as well as with and without illumination) can be found in Figure 2.11. When HMF was not present, water reduction occurred at the Ag_{gd} electrode

instead of HMF reduction. The anode reaction was always water oxidation. Since HMF reduction is more favorable than water reduction on the Ag_{gd} electrode, LSVs shift to the right both with and without illumination when HMF is present, meaning that smaller applied biases were required to generate the same level of current for HMF reduction.

Compared to currents generated in the dark, currents generated under illumination for both water reduction and HMF reduction require significantly decreased applied biases due to the photovoltage gained by the $BiVO_4$ photoanode under illumination. The results show that in order to achieve a current density of 1 mA/cm^2 for HMF reduction in the dark, an application of 2.41 V between the Ag_{gd} cathode and the $BiVO_4$/OEC anode was necessary. This voltage requirement is smaller by 0.35 V than that of the electrochemical cell where a Pt anode was used instead of a $BiVO_4$/OEC anode. This is because the OEC (i.e. FeOOH and NiOOH) coated on the $BiVO_4$ surface is more catalytic than Pt for water oxidation. When a PEC was used under AM 1.5G, 100 mW/cm^2 illumination, 1 mA/cm^2 was achieved at a potential of 0.92 V between the Ag_{gd} cathode and the $BiVO_4$/OEC anode, saving about 1.5 V.

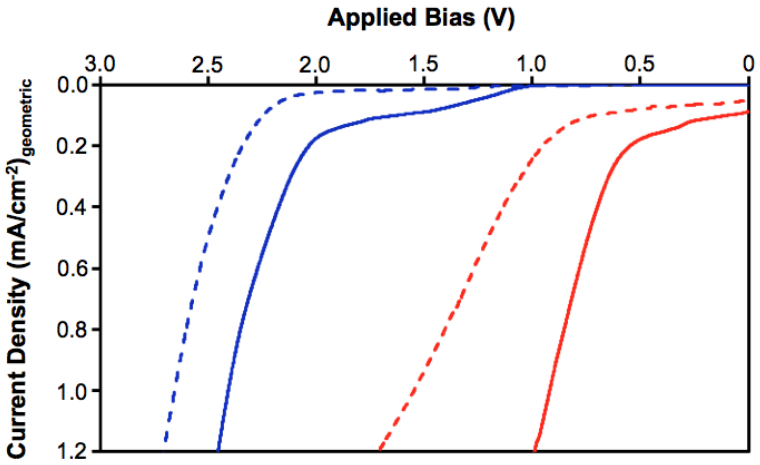

Figure 2.11. LSVs obtained using a two-electrode cell composed of a Ag_{gd} cathode and a $BiVO_4$/OEC anode in the dark (blue) and under AM 1.5G, 100 mW/cm^2 illumination (red) in a 0.5 M borate buffer (pH 9.2) with (solid) and without (dashed) 0.02 M HMF.

The reduction products, FE, and selectivity for photoelectrochemical reduction of HMF were analyzed after performing photoelectrochemical reduction at 1.0 V between the $BiVO_4$/OEC photoanode and the Ag_{gd} cathode (a two-electrode cell). It should be noted that this potential is not sufficient for electrochemical reduction of HMF using a two-electrode cell according to the LSVs shown in Figure 2.10c and Figure 2.11. The photoelectrochemical reduction results show that BHMF was produced with a FE of 94% and a selectivity of 95%, confirming that the results obtained from electrochemical HMF reduction can be reproduced by a PEC while decreasing the necessary electrical energy input. When better photoelectrodes (photoanode and/or photocathode) are developed with a smaller bandgap and a more negative CB position and the cell design is improved to minimize the IR drop within the cell, photoelectrochemical HMF reduction can be achieved with no external energy input.

This study demonstrated the use of a photoanode to construct a PEC. However, it will also be possible to construct a PEC by replacing the Ag cathode with a p-type semiconductor electrode (photocathode) when efficient and inexpensive p-type semiconductors that possess a proper CB position and stability around pH 9.2 are developed. In this case, the surface of photocathodes can be decorated with Ag catalysts to achieve BHMF production with high efficiency and selectivity.

2.4. Conclusions

In summary, electrochemical reduction conditions that can achieve selective HMF reduction to BHMF with the FE nearing 100% using Ag catalytic electrodes were identified. The Ag_{gd} electrode showed a wide potential region where hydrogenation of HMF can occur without inducing H_2 evolution. By systematically and thoroughly

analyzing potential-dependent FE and selectivity for BHMF production, optimum reduction conditions were identified and plausible hydrogenation mechanisms on the Ag surface were elucidated. The possibility of developing a PEC for HMF reduction by simply replacing a Pt anode with a $BiVO_4$ photoanode as a practical and inexpensive means to decrease the external voltage necessary for HMF reduction was also demonstrated, which provided one example of coupling solar energy conversion and biomass conversion.

The electrochemical and photoelectrochemical processes reported in this study offer practical and efficient routes for reductive biomass conversion, as they utilize water as the hydrogen source for hydrogenation without needing pre-formed H_2, eliminating multiple issues regarding the production, storage, and use of H_2. Similar approaches may be developed for other reductive biomass conversion processes.

2.5. References

1. G.W. Huber, S. Iborra, and A. Corma, *Chem. Rev.,* 2006, **106**, 4044-4098.
2. R. –J. van Putten, J. C. van der Waal, E. de Jong, C. B. Rasrendra, H. J. Heeres and J. G. de Vries, *Chem. Rev.,* 2013, **113**, 1499-1597.
3. A. A. Rosatella, S. P. Simeonov, R. F. M. Frade and C. A. M. Alfonso, *Green Chem.,* 2011, **13**, 754-793.
4. J. J. Bozell and G. R. Petersen, *Green Chem.,* 2010, **12**, 539-554.
5. J. Q. Bond, A. A. Upadhye, H. Olcay, G. A. Tompsett, J. Jae, R. Xing, D. M. Alonso, D. Wang, T. Zhang, R. Kumar, A. Foster, S. M. Sen, C. T. Maravelias, R. Malina, S. R. H. Barrett, R. Lobo, C. E. Wyman, J. A. Dumesic and G. W. Huber, *Energy Environ. Sci.,* 2014, **7**, 1500-1523.
6. G. W. Huber and J. A. Dumesic, *Catal. Today,* 2006, **111**, 119-132.
7. M. Balakrishnan, E. R. Sacia and A. T. Bell, *Green Chem.,* 2012, **14**, 1626-1634.
8. L. Cottier, G. Descotes and Y. Soro, *Synth. Commun.,* 2003, **33**, 4285-4295.
9. S. Goswami, S. Dey and S. Jana, *Tetrahedron,* 2008, **64**, 6358-6363.
10. V. Schiavo, G. Descotes and J. Mentech, *Bull. Soc. Chim. Fr.,* 1991, **128**, 704-711.
11. A. Faury, A. Gaset and J. P. Gorrichon, *Informations chimie,* 1981, **214**, 203-209.
12. R. Alamillo, M. Tucker, M. Chia, Y. Pagan-Torres and J. Dumesic, *Green Chem.,* 2012, **14**, 1413-1419.
13. J. Ohyama, A. Esaki, Y. Yamamoto, S. Arai and A. Satsuma, *RSC Adv.,* 2013, **3**, 1033-1036.
14. W. C. Albert and A. Lowy, *Trans. Electrochem. Soc*., 1939, 367-375.

15. K. G. Ellis, N. ul-Islam, D. W. Soper, J. H. P. Utley, H. L. Chum and M. Ratcliff, *J. Electrochem. Soc.*, 1987, **134**, 3058-3062.

16. Y. Kwon, E. de Jong, S. Raoufmoghaddam and M. T. M. Koper, *ChemSusChem,* 2013, **6**, 1659-1667.

17. P. Nilges and U. Schröder, *Energy Environ. Sci.,* 2013, **6**, 2925-2931.

18. Y. Kwon, Y. Y. Birdja, S. Raoufmoghaddam and M. T. M. Koper, *ChemSusChem,* 2015, **8**, 1745-1751.

19. N. S. Lewis, *Electrochem. Soc. Interface,* 2013, **22**, 43-49.

20. T. W. Kim and K. –S. Choi, *Science,* 2014, **343**, 990-994.

21. S. Swann Jr. *Ind. Eng. Chem.,* 1937, **29**, 1339-1341.

22. A. M. Couper, D. Pletcher and F. C. Walsh, *Chem. Rev*., 1990, **90**, 837-865.

23. F. Goodridge, K. Lister, R. E. Plimley and K. Scott, *J. Appl. Electrochem*. 1980, **10**, 55-60.

24. S. Trasatti, *J. Electroanal. Chem.,* 1972, **39**, 163-184.

25. P. Meakin, In *Fractals, Scaling and Growth Far from Equilibrium*; B. Chirikov, P. Cvitanovic, F. Moss and H. Swinney, Eds., Cambridge Univ. Press, Cambridge, UK, 1998, 326-400.

26. C. M. Lopez and K. –S. Choi, *Langmuir,* 2006, **22**, 10625-10629.

27. Y. Huang, S. Hu, S. Zuo, Z. Xu, C. Han and J. Shen, *J. Mater. Chem.,* 2009, **19**, 7759-7764.

28. B. E. Conway and M. Salomon, *Electrochim. Acta,* 1964, **9**, 1599-1615.

29. Y. Park, K. J. McDonald and K. –S. Choi, *Chem. Soc. Rev.,* 2013, **42**, 2321-2337.

30. R. S. Assary, P. C. Redfern, J. R. Hammond, J. Greeley, and L. A. Curtiss, *Chem. Phys. Lett.,* 2010, **497**, 123-128.

Chapter 3. Electrochemical Reductive Biomass Conversion: Direct Conversion of 5-hydroxymethylfurfural (HMF) to 2,5-hexanedione (HD) via Reductive Ring-opening

Portions of this chapter were published as:

J. J. Roylance and K. –S. Choi, *Green Chem.*, 2016, **18**, 2956-2960.

3.1. Introduction

Increasing concern over petroleum supply and climate change has driven the search for viable alternatives for our chemical and transportation fuel needs. Biomass has emerged as a leading contender due to its renewable nature and the vast number of compounds it can be used to generate, many of which have similar or improved properties to petroleum based counterparts.[1-12] HMF has become one of the most important biomass intermediates, being processed to a wide variety of important chemicals including transportation fuels (internal combustion, compression ignition, and jet engines), polymers, and pharmaceuticals.[1-15] Alternative transportation fuels have been of particular interest in recent years, with ethanol filling that role as a first generation biofuel. Concerns over its low energy content, high water solubility, and competition with food supply, among others, have led to the search for next generation biofuels.[9,10] DMF is one possible candidate due to its high octane number (119) and 40% higher energy content than ethanol, making it similar to gasoline, while being immiscible with water.[9,10]

Another alternative-fuel candidate is methylcyclopentane, which has a higher octane number and higher energy content than gasoline, and has fewer toxicity concerns than DMF.[11] It was recently demonstrated that methylcyclopentane can be produced from 2,5-hexanedione (HD), which is a hydrated form of DMF, by base-catalyzed intramolecular aldol condensation to 3-methylcyclopent-2-enone (MCP) followed by reduction (Figure 3.1a).[11] Aside from applications in alternative-fuels, HD can also be used to produce para-xylene, an important precursor in the production of terephthalic acid for polyethylene terephthalate (PET) (Figure 3.1a).[12] In addition, HD can be further reduced to 2,5-hexanediol, which has applications in

polymer synthesis, or to hexane (Figure 3.1a). This suggests that HD is a critical and versatile intermediate to form biofuels and building block chemicals.

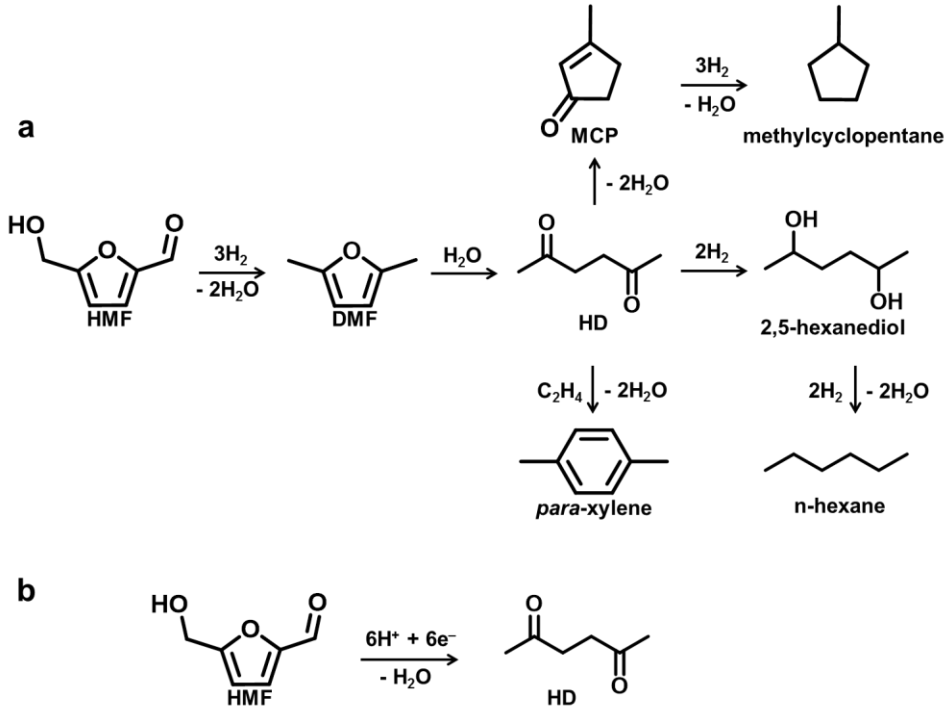

Figure 3.1. (a) Conventional production and potential use of HD and (b) direct electrochemical reduction of HMF to HD enabled by this study.

To date, conversion of HMF to HD has been achieved by reduction of HMF to DMF using precious metal catalysts and H_2 gas at high temperature and pressure, followed by ring opening via hydration (Figure 3.1a).[11,16,17] Here, the direct electrochemical reduction of HMF to HD using zinc as the catalytic electrode at ambient temperature and pressure is demonstrated (Figure 3.1b). This process does not require the use of H_2 gas or precious metals. Water (i.e. protons) is used as the hydrogen source without pre-reducing water to H_2 and HMF is directly converted to HD on the electrode surface without producing DMF. A few studies on

electrochemical reduction of HMF or furfural have been reported previously with the reduction of aldehyde group to alcohol being the most commonly observed reaction.[18-26] However, this study represents the first example of electrochemical reductive ring-opening of HMF with complete reduction of both the alcohol and the aldehyde groups.

3.2. Experimental

3.2.1. Materials

Zinc foil (0.25 mm thick, 99.98%) was purchased from Alfa Aesar. Copper foil was purchased from Nimrod Hall Copper Foil Company. Potassium phosphate, monobasic (≥ 99.0%) was purchased from Electron Microscopy Sciences. Potassium sulfate (≥ 99.0%), sulfuric acid (95-98%), phosphoric acid (≥ 85%), potassium hydroxide (≥ 85%), sodium acetate (≥ 99.0%), acetic acid (≥ 99.7%), 5-hydroxymethylfurfural (≥ 99%), 2,5-hexanedione (≥ 98%), and 5-methylfurfural (99%) were purchased from Sigma Aldrich. All chemicals were used without further purification.

3.2.2. Preparation of Electrodes

Zn and Cu electrodes used in this study were prepared by cutting Zn and Cu foil to pieces with dimensions of 1.5 cm x 2.5 cm. The Zn surface was mechanically polished with sandpaper. The Cu surface was first rinsed with 2-propanol and water, then cleaned by immersing in 1 M HCl for 1 minute to remove surface oxides. After rinsing with DI water and drying, Cu tape was attached to the Zn or Cu foil electrodes to enable connection to the potentiostat lead. The backside and top 0.5 cm of the Zn or Cu foil electrodes were then covered with Teflon tape to yield a 3.0 cm^2 working area. The cleaning and preparation of electrodes were performed immediately before use in experiments. The Au and Pt working electrodes (1.5 cm x 2.0 cm)

and Pt counter electrodes (2.5 cm x 2.0 cm) were prepared by sputter coating a 100 nm platinum or gold layer over a 20 nm titanium layer onto cleaned glass slides.

3.2.3. Reduction of HMF

LSVs were performed in a 0.2 M sulfate buffer solution (pH 2.0) with and without 0.02 M HMF in an undivided three-electrode cell without stirring. The potential was swept from the open circuit potential to the negative direction using a scan rate of 50 mV/s. The constant potential reduction of HMF was performed in a divided cell where the cathodic compartment and the anodic compartment were divided by a glass frit. The cathodic compartment contained 14 mL of a 0.2 M sulfate buffer solution (pH 2.0), a 0.2 M sulfate solution with pH adjusted to 1.0, a 0.2 M phosphate buffer solution (pH 2.0 and pH 7.2), or a 0.2 M acetate buffer solution (pH 4.7) commonly containing 0.02 M HMF while the anodic compartment contained the same solution without HMF. Reduction was performed by passing 20 C at various potentials discussed in section 3.3.

3.2.4. Product Analysis

Products were detected and quantified using a Bruker Avance III 400 MHz nuclear magnetic resonance (NMR) spectrometer. Calibration curves were generated for both HD and HMF by obtaining ^{1}H-NMR spectra for a series of solutions of known concentration for each species and plotting the area obtained for signature HMF and HD peaks for each concentration. The area for HMF and HD peaks of unknown concentrations from the product solution were then plotted against the calibration curves to determine their concentrations. The HMF signal in the product solution was also compared to that of the initial solution to determine the amount of HMF consumed. The identities of the products were further confirmed by ^{13}C-NMR, ^{1}H-^{13}C heteronuclear single quantum coherence (HSQC) spectroscopy, high pressure liquid

chromatography (HPLC), and gas chromatography-mass spectrometry (GCMS). HPLC was carried out using a Shimadzu Prominence-i LC-2030C HPLC with an ICSep ICE-COREGEL 87H3 column at 65 °C, 0.1 vol% H_2SO_4 in water mobile phase at 0.5 mL/min flow rate, and photo-diode array (PDA) and refractive index (RID) detectors. GCMS was carried out using a Shimadzu QP2010-Ultra equipped with He carrier gas, Aoc-20i+s autoinjector, split/splitless inlet, and a Shimadzu SHRIX5 column (30 m length, 0.25 mm diameter, 95% dimethylpolysiloxane 5% phenyl stationary phase).

3.3. Results and Discussion

The unique catalytic ability of Zn for electrochemical reduction of HMF to HD was first examined by comparing its LSVs for HMF reduction with those of Au, Cu, and Pt (Figure 3.2). For electrochemical reduction of HMF in aqueous media, water reduction to H_2 is the major competing reaction. Therefore, identifying good HMF reduction catalysts among poor H_2 evolution catalysts is necessary for achieving high FE for HMF reduction. Au and Cu were chosen as poor H_2 evolution catalysts and Pt was chosen as a good H_2 evolution catalyst to compare with the performance of Zn for HMF reduction.

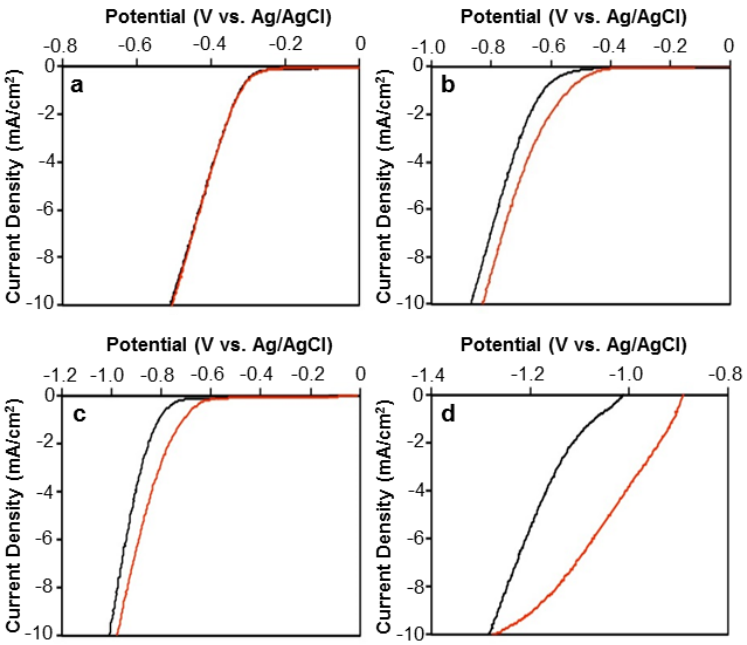

Figure 3.2. LSVs of (a) Pt, (b) Au, (c) Cu and (d) Zn electrodes in 0.2 M sulfate buffer (pH 2.0) with (red) and without (black) 0.02 M HMF (scan rate: 50 mV/s).

LSVs were performed in a 0.2 M sulfate buffer solution (pH 2.0) with and without 0.02 M HMF in an undivided three-electrode cell without stirring. The cathodic current shown in LSVs obtained before HMF was added is due to water reduction to H_2. As expected, Pt showed the most positive onset, followed by Au, Cu, and Zn. When HMF was added, Pt did not show a change either in the onset potential or in current profile, because water reduction is dominant on the Pt surface whether or not HMF is present. In the case of Au and Cu, the onset potential for reduction current was shifted to the positive direction by 50-100 mV when HMF was present, suggesting HMF reduction occurs before H_2 evolution on these electrodes. The most significant change in onset potential and current profile when HMF was added was observed for Zn, which demonstrated a current density of more than 4 mA/cm2 for HMF reduction at the potential where water reduction initiates.

The reduction products and conversion efficiencies for HMF reduction were analyzed by performing HMF reduction in a divided cell at a constant potential of -1.2 V vs. Ag/AgCl (equivalent to -0.89 V vs. RHE) by passing 20 C in 14 mL of a 0.2 M sulfate buffer solution (pH 2.0) containing 0.02 M HMF. It should be noted that the reduction of HMF to HD consumes protons (Figure 3.1b). Therefore, the local pH at the working electrode will rapidly rise during the course of electrolysis if an unbuffered weakly acidic solution is used. This pH change can constantly vary the yield, selectivity, and the type of product throughout the electrolysis. Therefore, in order to accurately evaluate the pH effect, it is critical to use a buffered solution to obtain results at a constant pH of interest. After reduction, the electrolyte was analyzed by ^{1}H-NMR to quantify the products (Figure 3.3). Based on these results, FE and selectivity for HD formation were calculated using equations 3.1 and 3.2, where F is the Faraday constant (96485 C/mol) and n is the number of electrons required for the conversion of an HMF molecule to an HD molecule, which is 6. The results are summarized in Table 3.1.

$$\text{FE}\ (\%) = \frac{\text{mol of HD formed}}{\text{Total charge passed (C)}/\ (\text{F}\times\text{n})} \times 100\% \qquad (3.1)$$

$$\text{Selectivity of HD}\ (\%) = \frac{\text{mol of HD formed}}{\text{mol of HMF consumed}} \times 100\% \qquad (3.2)$$

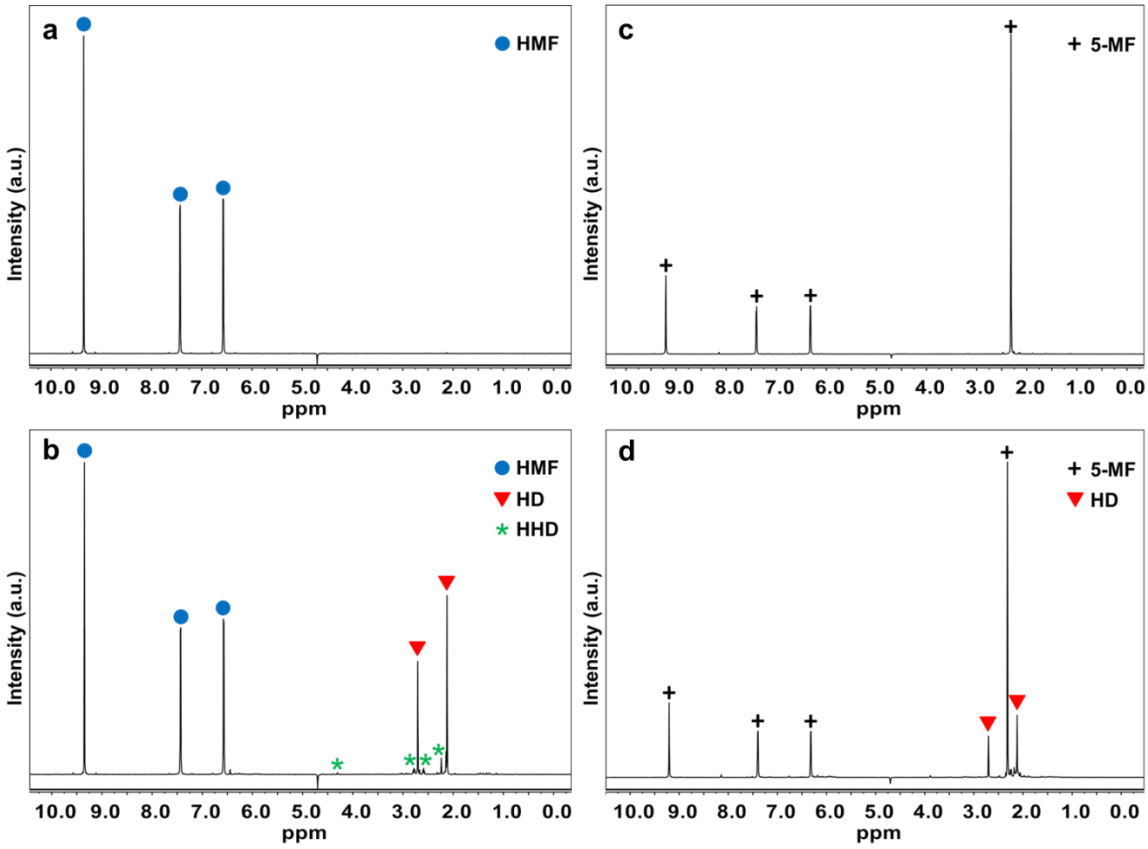

Figure 3.3. (a-b) ^{1}H-NMR spectra for a 0.2 M sulfate buffer solution (pH 2.0) containing 0.02 M HMF (a) before and (b) after passing 20 C at –1.2 V vs. Ag/AgCl to the Zn electrode for HMF reduction. ^{1}H NMR (400 MHz, 90% H_2O/ 10% D_2O): δ 9.35 (s, 1H), 7.43 (d, *J* = 3.9 Hz, 1H), 6.57 (d, *J* = 3.9 Hz, 1H), 4.31 (s, 2H), 2.78 (t, *J* = 6.3 Hz, 2H), 2.71 (s, 4H), 2.59 (t, *J* = 6.3 Hz, 2H), 2.24 (s, 3H), 2.12 (s, 6H); (c-d) ^{1}H-NMR spectra for a 0.2 M sulfate buffer solution (pH 2.0) containing 0.02 M 5-MF (c) before and (d) after passing 20 C at -1.2 V vs. Ag/AgCl to the Zn electrode for 5-MF reduction. ^{1}H NMR (400 MHz, 90% H_2O/ 10% D_2O): δ 9.21 (s, 1H), 7.40 (d, *J* = 3.9 Hz, 1H), 6.32 (d, *J* = 3.8 Hz, 1H), 2.70 (s, 4H), 2.32 (s, 3H), 2.12 (s, 6H).

(HMF peaks at 9.35, 7.43, and 6.57 ppm. HD peaks at 2.71 and 2.12 ppm. HHD peaks at 4.31, 2.78, 2.59, and 2.24 ppm. 5-MF peaks at 9.21, 7.40, 6.32, and 2.32 ppm. The HHD peak at 4.31 ppm is diminished by water suppression.)

Table 3.1. Electrochemical reduction of HMF by Pt, Au, Cu and Zn electrodes.[a]

Electrode	Pt	Au	Cu	Zn
Average Current Density (mA/cm^2)	57.4	50.1	39.6	14.4
HMF consumed (μmol)	5.01	11.9	16.0	30.6
HD formed (μmol)	0	0.826	1.30	25.0
BHMF formed (μmol)	5.00	5.10	6.32	0.978
HHD formed (μmol)	0	0.823	1.98	2.75
FE for HD (%)	0	2.39	3.75	72.4
Selectivity for HD (%)	0	6.92	8.13	81.6

[a] Reaction conditions: E = –1.2 V vs. Ag/AgCl (= –0.89 V vs. RHE) in a 0.2 M sulfate buffer (pH 2.0) containing 0.02 M HMF for 20 C passed.

As expected, H_2 production was the major reaction on Pt; only a small amount of HMF was converted to BHMF (FE = 4.83%) and no HD was detected. In the case of Au and Cu, a slightly larger fraction of charges were used for BHMF production (FE = 4.92% and 6.10% for Au and Cu, respectively). HD was also detected as a reduction product, but FE for HD production was below 4%. Surprisingly, Zn electrodes produced HD at high efficiency (FE = 72.4%) and selectivity (81.6%) with only a trace amount of BHMF (FE < 1%). Hydroxy-2,5-hexanedione (HHD) was also detected as a byproduct (FE = 5.64%). The reduction of HMF to BHMF, HD, and HHD requires $2e^-$, $6e^-$, and $4e^-$, respectively as the reaction schemes show in Figure 3.4a. DMF was not detected, suggesting that the electrochemical conversion of HMF to HD does not involve the formation of DMF.

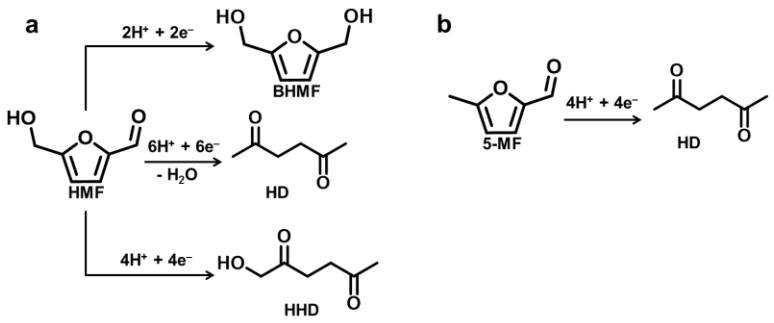

Figure 3.4. Electrochemical reduction products of (a) HMF and (b) 5-MF on Zn at -1.2 V vs. Ag/AgCl in a 0.2 M sulfate buffer solution (pH 2.0) containing 0.02 M HMF.

The potential dependence of HD production by Zn in the same solution was investigated and the results are summarized in Table 2. The highest FE (72.4%) was achieved at -1.2 V vs. Ag/AgCl. Applying more negative potentials (E < -1.4 V vs. Ag/AgCl) decreased FE for HD production because water reduction became more favorable on the Zn surface in the high overpotential region. When a more positive potential than -1.2 V was applied, FE did not change significantly, but the average current decreased, which decreased the rate for HD production.

Table 2. Electrochemical reduction of HMF by Zn at various potentials.[a]

E (V) vs. Ag/AgCl	-1.0	-1.2	-1.4	-1.6
Average Current Density (mA/cm^2)	6.27	14.4	20.4	39.2
HD formed (μmol)	23.4	25.0	22.7	12.9
FE (%)	67.6	72.4	65.8	37.4
Selectivity (%)	77.6	81.6	79.5	60.6

[a] Reaction conditions: 0.2 M sulfate buffer (pH 2.0) containing 0.02 M HMF for 20 C passed.

The conversion of HMF to HD on Zn demonstrates a strong dependence on solution pH. When the pH of the sulfate solution was lowered to 1, HD was still produced but the FE for HD production decreased (FE = 50.7% at -1.2 V vs. Ag/AgCl for a pH 1.0 sulfate buffer solution) because water reduction became more favorable at a lower pH. On the other hand, when the pH was increased to 7.2 (0.2 M phosphate buffer), no HD was formed and the major product was BHMF (57.7 % FE at -1.7 V vs. Ag/AgCl). To confirm that this is truly due to the pH effect and not due to the anion effect (phosphate vs. sulfate) the same reduction reaction was performed in a pH 2.0 solution using a phosphate buffer, which produced HD at efficiencies that were equivalent to those in sulfate (pH 2.0). When a midpoint pH was tested using a 0.2 M acetate buffer (pH 4.7), HD was still formed but the FE dropped to 28% at -1.2 V vs. Ag/AgCl along with a corresponding increase in the production of BHMF. Therefore, pH 2 was identified as an optimum pH to produce HD.

Since HD is a hydrated open ring structure of DMF, the conversion of HMF to HD is in essence composed of three steps: hydrogenolysis (i.e. replacement of the alcohol group with a terminal hydrogen), the conversion of the formyl group to a terminal alkane, and ring opening. It is believed that the unique ability of Zn to produce HD by HMF reduction is related to the well-known ability of Zn to perform the Clemmensen reduction, which reduces aldehydes or ketones to the corresponding hydrocarbon, consuming 4 protons and 4 electrons with a removal of one H_2O (Figure 3.5a).[27]

The fact that DMF was not detected as a byproduct or an intermediate suggests that for electrochemical HMF reduction on Zn in an acidic medium, the formation of DMF and the hydrolysis of DMF to HD do not occur in a decoupled sequential manner. Rather, acid catalyzed ring opening of a furan ring and Clemmensen reduction occur in a concerted manner, resulting in

direct reductive ring opening of HMF to HD. However, the mechanism for opening of the furan ring should still be similar to those well established for other furan rings, which commonly involve the ring opening between C2 and the furan oxygen by a nucleophilic attack from water.[28-30] The ring opening of DMF to HD is shown in Figure 3.5b as an example.[30] Consequently, one carbonyl oxygen of HD is from the furan oxygen and the other carbonyl oxygen is from water.

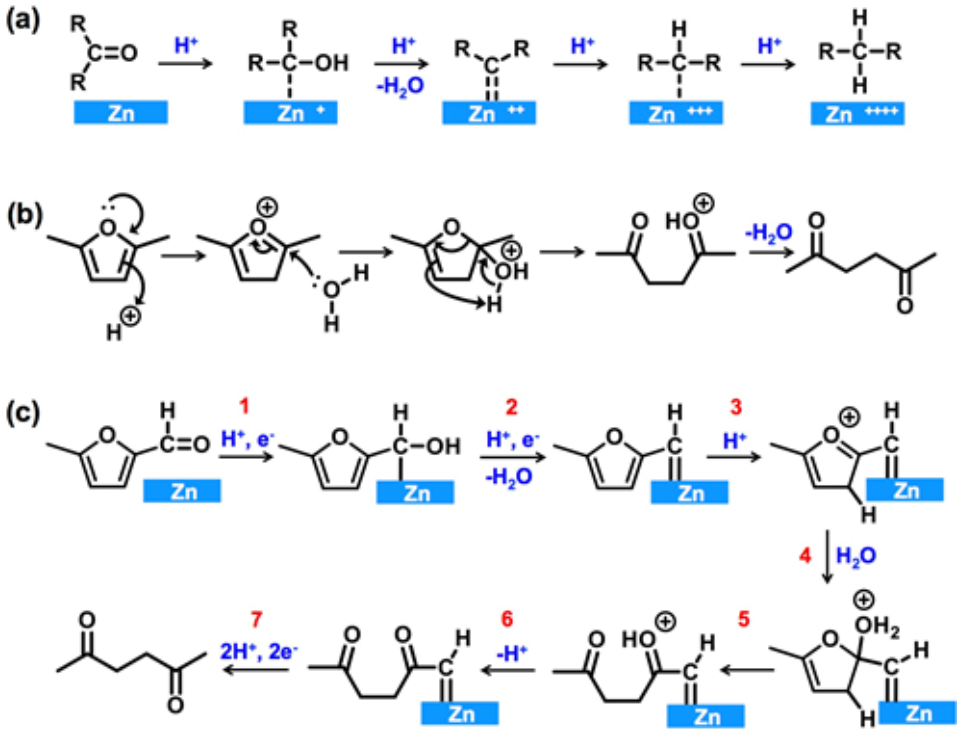

Figure 3.5 (a) A general mechanism of Clemmensen reduction on Zn. Zn is used as the electron source and the (+) charges on Zn represent how many electrons are used in each step; (b) a ring-opening mechanism of DMF to HD by hydrolysis; (c) a predictive model for the reduction of 5-MF to HD constructed by combining mechanisms shown in (a) and (b).

A key remaining question in proposing a mechanism for the reduction of HMF to HD is when the hydrogenolysis of HMF occurs (e.g. before, during, or after Clemmensen reduction). In order to examine whether the hydrogenolysis step of HMF is critical for reductive ring opening, we performed the reduction of 5-methylfurfural (5-MF) on Zn using the same reduction conditions (Figure 3.4b). 5-MF is an analogous compound of HMF having a furan ring and a formyl group, but without an alcohol group. The result shows that the same HD was obtained as the only detectable HMF reduction product (FE = 38.3%). The fact that the absence of the alcohol group does not affect the reductive ring-opening process of the furan ring suggests that the hydrogenolysis of HMF to 5-MF is an independent step from reductive ring opening and it most likely occurs before reductive ring opening.

By combining Clemmensen reduction and ring-opening mechanisms, a predictive model for the reduction of 5-MF to HD on the Zn surface is proposed in Figure 3.5c. The resemblance of the predictive model to Clemmensen reduction and ring-opening mechanisms can be easily seen by comparing Figure 3.5c with Figures 3.5a and 3.5b, where Steps 1, 2, 3, and 7 are associated with Clemmensen reduction while steps 4-6 are associated with ring opening. As in the case of the conversion of DMF to HD, one carbonyl oxygen of HD is from the furan oxygen of 5-MF and the other carbonyl oxygen is from water while the formyl group of 5-MF is converted to the terminal alkyl group by Clemmensen reduction. In the conventional Clemmensen reduction Zn serves as the electron source and is oxidized to Zn^{2+}. However, in an electrochemical cell, electrons are provided from the half reaction occurring at the anode (water oxidation). Therefore, the catalytic surface of Zn is not oxidized during the reduction process. SEM images of the Zn electrode before and after the HMF reduction are shown in Figure 3.6. After HMF reduction, the Zn surface was roughened, suggesting that the Zn surface was

restructured during the catalytic reaction by HMF-Zn interactions. Comparing images shown in Figures 3.6a and 3.6b, a Zn electrode before and after passing 20 C for electrochemical reduction of HMF at -1.2 V vs Ag/AgCl in a 0.2 M sulfate buffer solution (pH 2.0), suggests that surface restructuring of Zn occurs during HMF reduction. However, the fact that the surface morphologies of Zn after passing 20 C and 40 C, shown figure 3.6c, are comparable suggests that after initial restructuring of the surface, continuous alteration of the surface does not occur. The Zn surface after passing 20 C at the same potential without the presence of HMF in solution, shown in Figure 3.6d, looks comparable to the fresh Zn surface, confirming that the surface roughening is due to the interactions between the Zn surface and HMF under reduction conditions and not simply due to the application of potential for reduction or other factors such as water reduction.

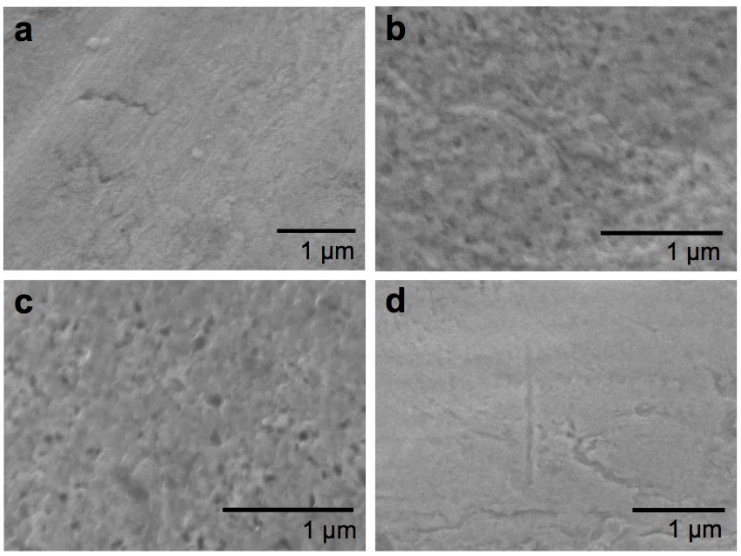

Figure 3.6. SEM images of (a) a Zn electrode before electrochemical reduction, a Zn electrode after passing (b) 20 C and (c) 40 C at -1.2 V vs. Ag/AgCl (-0.89 V vs. RHE) in a 0.2 M sulfate buffer solution (pH 2.0) containing 0.02 M HMF, (d) a Zn electrode after passing 20 C at the same potential in the same solution that did not contain HMF.

A plausible mechanism for the reduction of HMF to HD is also shown in Figure 3.7 where hydrogenolysis of HMF precedes ring opening and the remaining reduction steps are exactly the same as those shown for the reduction of 5-MF. As mentioned earlier, HMF reduction also produced a small amount of HHD, which was not detected from reduction of 5-MF. This can be explained by the possibility that a small fraction of HMF goes through reductive ring opening without going through hydrogenolysis first. A plausible mechanism for this pathway is also shown in Figure 3.7. In this case, the final ring-opened product, HHD, would still contain the alcohol group from HMF. While the conversion of HMF to HD requires 6 electrons and 6 protons with a loss of one H_2O, the conversion of 5-MF to HD and the conversion of HMF to HHD, which do not involve hydrogenolysis, both require only 4 electrons and 4 protons. The relationship between the reduction processes of these three reactions is demonstrated in Figure 3.7.

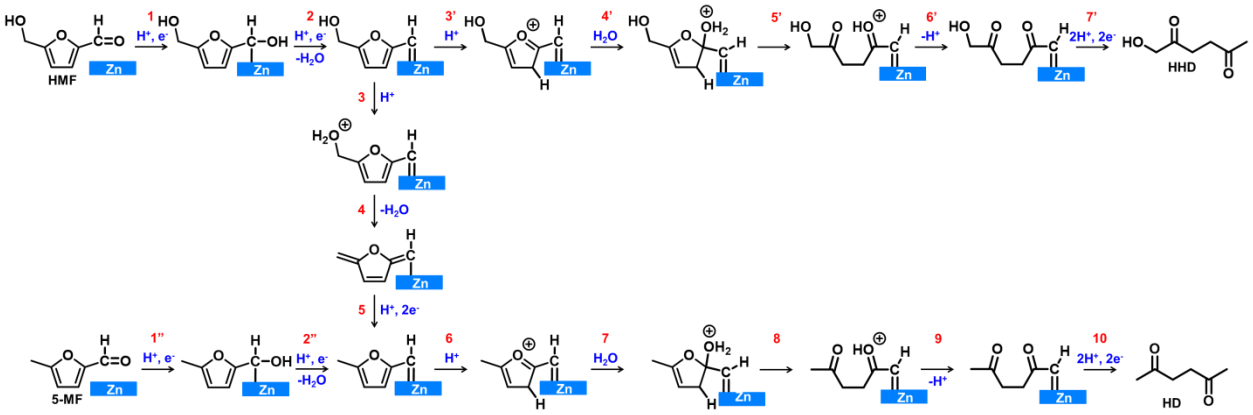

Figure 3.7. A plausible mechanism for the electrochemical reduction of HMF to HD on Zn electrodes composed of hydrogenolysis (steps 3-5) and reductive ring opening (steps 6-10). The scheme also shows the reduction of HMF to HHD (top row) and the reduction of 5-MF to HD (bottom row), which involve only reductive ring opening without hydrogenolysis, to demonstrate how these reaction pathways are related to one another.

3.4. Conclusion

In summary, it was demonstrated that Zn electrodes have the unique ability to electrochemically convert HMF to HD in acidic aqueous media under ambient condition using only water as the H source. The overall reaction is composed of hydrogenolysis and Clemmensen reduction coupled with furan ring opening. FE and selectivity as high as 72.4% and 81.6%, respectively, were achieved for HMF reduction at -1.2 V vs. Ag/AgCl in a pH 2 solution, which was an optimal condition to suppress H_2 evolution and the conversion of HMF to BHMF. Comparing the reduction of HMF and 5-MF on Zn, a plausible mechanism for the formation of HD and HHD were proposed. The unique reduction pathway that can directly convert HMF or 5-MF to HD reported in this study will serve as a new route to valorize biomass intermediates.

3.5. References

1. G. W. Huber, S. Iborra and A. Corma, *Chem. Rev.*, 2006, **106**, 4044-4098.
2. R.-J. van Putten, J. C. van der Waal, E. de Jong, C. B. Rasrendra, H. J. Heeres and J. G. de Vries, *Chem. Rev.*, 2013, **113**, 1499-1597.
3. A. Rosatella, S. P. Simeonov, R. F. M. Frade and C. A. M. Alfonso, *Green Chem.*, 2011, **13**, 754-793.
4. J. J. Bozell and G. R. Petersen, *Green Chem.*, 2010, **12**, 539-554.
5. J. Q. Bond, A. A. Upadhye, H. Olcay, G. A. Tompsett, J. Jae, R. Xing, D. M. Alonso, D. Wang, T. Zhang, R. Kumar, A. Foster, S. M. Sen, C. T. Maravelias, R. Malina, S. R. H. Barrett, R. Lobo, C. E. Wyman, J. A. Dumesic and G. W. Huber, *Energy Environ. Sci.*, 2014, **7**, 1500-1523.
6. G. W. Huber and J. A. Dumesic, *Catal. Today*, 2006, **111**, 119-132.
7. M. Balakrishnan, E. R. Sacia and A. T. Bell, *Green Chem.*, 2012, **14**, 1626-1634.
8. J. M. R. Gallo, D. M. Alonso, M. A. ; Mellmer and J. A. Dumesic, *Green Chem.*, 2013, **15**, 85-90.
9. J. B. Binder and R. T. Raines, *J. Am. Chem. Soc.*, 2009, **131**, 1979-1985.
10. Y. Roman-Leshkov, C. J. Barrett, Z. Y. Liu and J. A. Dumesic, *Nature*, 2007, **447**, 982-986.
11. E. Sacia, M. Deaner, Y. Louie and A. Bell, *Green Chem.*, 2015, **17**, 2393-2397.
12. M. Masuno, P. Smith, D. Hucul, K. Brune, R. Smith, J. Bissell, D. Hirsch-Weil and E. Stark, US Patent No. 8889938 B2, Nov. 18, 2014.
13. W. –H. Peng, Y. –Y. Lee, C. Wu and K. C. –W. Wu, *J. Mater. Chem.*, 2012, **22**, 23181-23185.

14. M. I. Alam, S. De, B. Singh, B. Saha and M. M. Abu-Omar, *Appl. Catal., A*, 2014, **468**, 42-48.

15. Y. –C. Lee, S. Dutta and K. C. –W. Wu, *ChemSusChem*, 2014, **7**, 3241-3246.

16. M. Chidambaram and A. T. Bell *Green Chem.*, 2010, **12**, 1253-1262.

17. F. Liu, M. Audemar, K. D. E. Vigier, J.-M. Clacens, F. De Campo and F. Jérôme, *ChemSusChem*, 2014, **7**, 2089-2095.

18. Y. Kwon, E. de Jong, S. Raoufmoghaddam and M. T. M. Koper, *ChemSusChem*, 2013, **6**, 1659-1667.

19. P. Nilges and U. Schröder, *Energy Environ. Sci.*, 2013, **6**, 2925-2931.

20. Y. Kwon, Y. Y. Birdja, S. Raoufmoghaddam and M. T. M. Koper, *ChemSusChem*, 2015, **8**, 1745-1751.

21. J. J. Roylance, T. W. Kim and K. –S. Choi, *ACS Catal.*, 2016, **6**, 1840-1847.

22. S. K. Green, J. Lee, H. J. Kim, G. A. Tompsett, W. B. Kim and G. W. Huber, *Green Chem.*, 2013, **15**, 1869-1879.

23. G. Chamoulaud, D. Floner, C. Moinet, C. Lamy and E. M. Belgsir, *Electrochim. Acta*, 2001, **46**, 2757-2760.

24. P. Parpot, A. P. Bettencourt, G. Chamoulaud, K. B. Kokoh and E. M. Belgsir, *Electrochim. Acta*, 2004, **49**, 397-403.

25. Z. Li, S. Kelkar, C. H. Lam, K. Luczek, J. E. Jackson, D. J. Miller and C. M. Saffron, *Electrochim. Acta*, 2012, **64**, 87-93.

26. B. Zhao, M. Chen, Q. Guo and Y. Fu, *Electrochim. Acta*, 2014, **135**, 139-146.

27. J. H. Brewster, *J. Am. Chem. Soc.*, 1954, **76**, 6364-6368.

28. J. Horvat, B. Klaic, B. Metelko and V. Sunjic, *Tetrahedron Lett.*, 1985, **26**, 2111-2114.

29. V. Schiavo, G. V. Descotes and J. Mentech, *J. Bull. Soc. Chim. Fr.*, 1991, **128**, 704-711.

30. N. Nikbin, S. Caratzoulas and D. G. Vlachos, *ChemSusChem*, 2013, **6**, 2066-2068.

Chapter 4. Electrochemical Reductive Amination of Furfural-Based Biomass Intermediates

4.1. Introduction

Among the many reactions HMF may undergo, reductive amination, which adds an amine group to a hydrocarbon framework, enables the synthesis of more diverse biomass-driven compounds including amine-based polymers (nylon) and pharmaceutical compounds.[1-6] Reductive amination of furfurals involves the conversion of the formyl group to an amine group, which is commonly accomplished in two steps as illustrated in Figure 4.1.[6-8] In this scheme the aldehyde is first converted to an aldimine (Step 1 in Figure 4.1) by reaction with ammonia or a primary amine. Formation of the aldimine has traditionally utilized concentrated or liquid amine source and nonaqueous solvents.[9-12] However, aldmine can also be formed in aqueous media under pH conditions where a large portion of ammonia or amine is present in its unprotonated form.[13,14] The stability of aldmine is pH dependent and lowering pH can cause the hydrolysis of the aldimine back to aldehyde.[12]

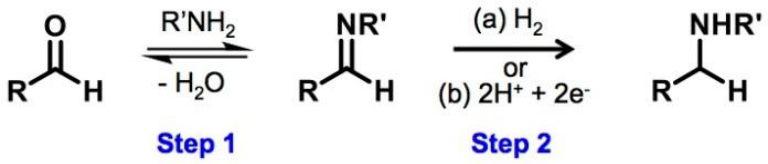

Figure 4.1. The general reductive amination pathway. Step 1: formation of an aldimine by reaction of an aldehyde and a primary amine. Step 2: reduction either (a) by hydrogenation using H_2 as the hydrogen source or (b) by hydrogenation using H^+ from H_2O as the hydrogen source accompanied by an electron source.

The second step of reductive amination is reduction of the aldimine to an amine by the hydrogenation of the C=N bond (Step 2 in Figure 4.1). This process has commonly been achieved by using H_2 over Raney Ni or precious metal catalysts (e.g. Au, Ir, Pd, Pt, Rh, and

Ru).[5,8,10,15,16] Recent efforts have been made to utilize inexpensive alternatives, such as FeNi alloy catalysts.[7] However, for this method H_2, which is a valuable fuel that must be generated from other primary energy sources, needs to be consumed. Hydrogenation can also be achieved by using a hydride (e.g. sodium borohydride, sodium cyanoborohydride, and sodium triacetoxyborohydride)[6,15,17] or by using Zn powder as a reducing agent and water as the hydrogen source.[12,14] These reactions, however, require the consumption of reducing agents, significant solution cleanup, and disposal of waste that can be toxic.

Electrochemical reductive amination can offer an attractive alternative approach by using water as the hydrogen source without requiring other chemicals as the reducing agent, providing reaction conditions that are more environmentally benign. However, few studies have been reported previously for electrochemical reductive amination, utilizing substrates such as cyclohexanone and derivatives, acetone, hexanal, and 2,5-hexanedione.[13,18-21] These studies commonly used mercury or lead electrodes which are known to have high overpotentials for the hydrogen evolution reaction, the main competing reaction for reductive amination. No systematic attempts on identifying optimum substrate types for catalytic electrodes in terms of increasing FE or minimizing overpotential necessary for reductive amination were made to date. It would be highly beneficial to identify optimum non-toxic catalytic electrodes and operating conditions to perform reductive amination in aqueous media without a significant loss of FE to water reduction.

In this study, the catalytic abilities of various metal electrodes (Ag, Cu, Pt, Sn, and Zn) for reductive amination of HMF with methylamine were investigated and compared. For each metal electrode, potentials necessary to initiate reductive amination as well as potential dependent FE were investigated systematically. It was discovered that Ag and Zn electrodes

show an exceptional ability for reductive amination of HMF. Based on these results, optimum electrodes and reduction conditions that can achieve a FE and a selectivity nearing 100% are reported. The reductive amination of HMF derivatives such as 5-MF, 2,5-diformylfuran (DFF), and 5-formyl-2-furancarboxylic acid (FFCA) using methylamine as well as reductive amination of HMF using ethanolamine ($HOCH_2CH_2NH_2$) is also demonstrated to establish electrochemical reductive amination as a general route for reductive amination of furfural-based biomass intermediates.

4.2. Experimental

4.2.1. Materials

Zinc foil (0.25 mm thick, 99.98%), Sn foil (0.025 mm thick, 99.9%), and silver nitrate (99.9+%) was purchased from Alfa Aesar. Copper foil (1 Mil, 0.001 in. thick, 99.9%) was purchased from Nimrod Hall Copper Foil Company. Sulfuric acid (95-98%), methylamine (40 wt%), ethanolamine (> 99%), 5-hydroxymethylfurfural (≥ 99%), 5-methylfurfural (99%), dimethylsulfone,(98%), and sodium acetate (≥ 99.0%) were purchased from Sigma Aldrich. 2,5-diformylfuran (> 98%) and 5-formyl-2-furancarboxylic acid (> 98%) were purchased from TCI. All chemicals were used without further purification.

4.2.2. Preparation of Electrodes

Cu, Sn, and Zn electrodes used in this study were prepared by cutting the foil to pieces with dimensions of 1.5 cm x 2.5 cm. The Zn surface was mechanically polished with sandpaper. The Cu and Sn surfaces were first rinsed with 2-propanol and water, then cleaned by immersing in 1 M HCl for 1 minute to remove surface oxides. After rinsing with DI water and drying, Cu tape was attached to the foil electrodes to enable connection to the potentiostat lead. The backside and top 0.5 cm of the foil electrodes were then covered with Teflon tape to yield a 3.0

cm^2 working area. The cleaning and preparation of electrodes were performed immediately before use in experiments. Ag_{sp} and Ag_{gd} electrodes (1.5 cm x 2.5 cm) were prepared following the method described in section 2.2.2. The Pt working (1.5 cm x 2.0 cm) and counter electrodes (2.5 cm x 2.0 cm) were prepared following the method describe in section 3.2.2.

4.2.3. Solution Preparation and Aldimine formation

The 0.7 M methylamine buffer solution was prepared by diluting concentrated aqueous CH_3NH_2 (pK_a = 10.6) with ultrapure water and acidifying to pH 11.0 with concentrated H_2SO_4. The necessary amount of HMF, 5-MF, DFF, or FFCA was added to make a 0.02 M solution. The same procedure was followed for reaction of HMF with ethanolamine ($HOCH_2CH_2NH_2$), where the solution was prepared with ethanolamine instead of methylamine. Although the pK_a (9.5) of ethanolamine is lower than that of methylamine, the pH of the ethanolamine solution was adjusted to 11.0 to be consistent with the pH of the methylamine solution used in this study.

4.2.4. Reduction of HMF

LSVs were performed in a 0.7 M methylamine buffer solution (pH 11.0) with and without 0.02 M HMF in an undivided three-electrode cell without stirring. The potential was swept from the open circuit potential to the negative direction using a scan rate of 5 mV/s. The constant potential reduction of HMF was performed in a divided cell where the cathodic compartment and the anodic compartment were divided by a glass frit. The cathodic compartment contained 14 mL of the buffer solution (pH 11.0) with 0.02 M HMF while the anodic compartment contained the same solution without HMF. Reduction was performed by passing 20 C (or the desired coulombs) at various potentials. The FE and selectivity of each reaction were calculated using equations 4.1 and 4.2, where F is the Faraday constant (96485

C/mol) and n is the number of electrons required for the conversion of the aldimine to an amine, which is 2 for all substrates except DFF, where n=4.

$$\text{FE}\ (\%) = \frac{\text{mol of amine formed}}{\text{Total charge passed (C)}/\ (\text{F}\times\text{n})} \times 100\% \qquad (4.1)$$

$$\text{Selectivity}\ (\%) = \frac{\text{mol of amine formed}}{\text{mol of HMF consumed}} \times 100\% \qquad (4.2)$$

4.2.5. Product Analysis

Products were detected and quantified via ^{1}H nuclear magnetic resonance (NMR) spectroscopy using a Bruker Avance III 400 MHz NMR spectrometer. An internal standard of dimethyl sulfone or sodium acetate was used to determine product concentrations. The HMF signal in the product solution was also compared to that of the initial solution to determine the amount of HMF consumed. The identities of the products were further confirmed by ^{13}C-NMR, and ^{1}H-^{13}C HSQC. Since the water suppression method used to analyze the sample also results in a suppression of the signals near water (4.7 ppm), the product was extracted with $CDCl_3$ and analyzed to confirm peak assignments and product identification.

4.3. Results and Discussion

A 0.7 M aqueous methylamine buffer solution (pH 11.0) containing 20 mM HMF, was prepared for electrochemical reductive amination. Aldimine formation is pH sensitive because amines go through base dissociation reaction in aqueous media and only the unprotonated base form of amine can undergo aldimine formation (Step 1 in Figure 4.2). Since the pK_a of $CH_3NH_3^+$ is ~10.6, adjusting the solution pH to 11.0 ensures a significant portion of amine to be present as a base form (0.5 M) to react with HMF to form aldimine. An NMR spectrum of 20

mM HMF in a methylamine solution (pH 11.0) shows all HMF in this solution is converted to aldimine (Figure 4.3a). When the pH was lowered to 9.0 or 7.0, the acid-base equilibrium of amine was shifted, resulting in hydrolysis of the aldimine to the aldehyde. As a result, HMF was recovered to near completion by pH 7.0 (Figure 4.3b-c).

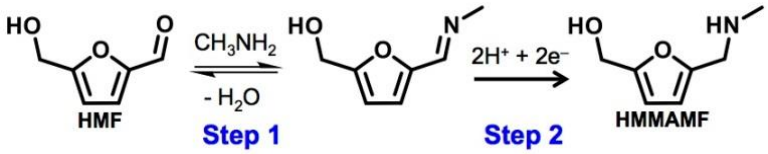

Figure 4.2. Electrochemical reductive amination of HMF. Reversible formation of an aldimine by reaction of the formyl group in HMF with CH_3NH_2 in step 1 followed by electrochemical hydrogenation using H^+ from H_2O as the hydrogen source in step 2.

The reduction of the aldimine to the amine product, 2-hydroxymethyl-5-(methylaminomethyl)furan (HMMAMF) (Step 2 in Figure 4.2) was first examined by performing LSVs using Ag_{sp}, Cu, Pt, Sn, and Zn metal electrodes in a methylamine solution with and without 20 mM HMF (Figure 4.4). In order to maximize FE for reductive amination, metals that are known to be poorly catalytic for water reduction were investigated, except for Pt, which was chosen to serve as a control electrode. Cathodic current generated in the absence of HMF can be attributed to water reduction to H_2 as there is no other species that are reductively active. Changes to the current profile upon addition of HMF, particularly a shift in current onset to the positive direction can be considered an indication that reductive amination of HMF is favored over water reduction.

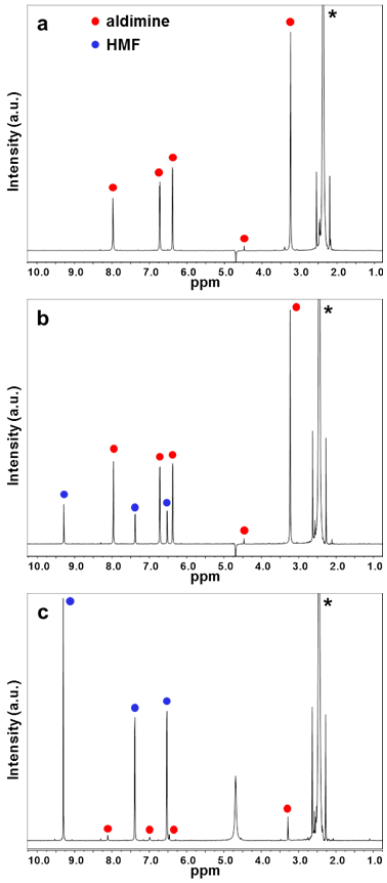

Figure 4.3. (a) ^{1}H-NMR spectrum for a 0.02 M HMF solution in 0.7 M methylamine at pH 11.0, ^{1}H NMR (400 MHz, 90% H_2O/ 10% D_2O) δ 7.97 (s, 1H), 6.73 (d, *J* = 3.4 Hz, 1H), 6.38 (d, *J* = 3.6 Hz, 1H), 4.48 (s, 1H), 3.24 (s, 3H), all peaks from aldimine. (b) ^{1}H-NMR spectrum for the pH 11 solution acidified to pH 9.0 showing partial recovery of HMF, ^{1}H NMR (400 MHz, 90% H_2O/ 10% D_2O): δ 9.29 (s, 1H), 7.96 (s, 1H), 7.38 (d, *J* = 3.8 Hz, 1H), 6.72 (d, *J* = 3.6 Hz, 1H), 6.52 (d, *J* = 3.9 Hz, 1H), 6.37 (d, *J* = 3.5 Hz, 1H), 4.47 (s, 1H), 3.23 (s, 3H). HMF peaks at 9.29, 7.38, and 6.52, aldimine peaks at 7.96, 6.72, 6.37, 4.47, and 3.23. (c) ^{1}H-NMR spectrum for the pH 11 solution acidified to pH 7.0 showing nearly complete recovery of HMF, ^{1}H NMR (400 MHz, 90% H_2O/ 10% D_2O): δ 9.30 (s, 1H), 7.39 (d, *J* = 3.8 Hz, 1H), 6.53 (d, *J* = 3.8 Hz, 1H), 6.37 (d, *J* = 3.5 Hz, 1H). HMF peaks at 9.30, 7.39, and 6.53 ppm. Minor aldimine peaks at 8.11, 6.99, 6.47, and 3.28. The aldimine peak near 4.48 ppm is diminished by water suppression, which is present as the peak (or inverted peak in c) at 4.70 ppm. The peak denoted by * is from methylamine.

The LSVs obtained for a Pt electrode with and without HMF are shown in Figure 4.4a. When HMF was added, the cathodic onset was shifted to the negative direction with a decrease in current density. This suggests that reduction of aldimine is not favored over water reduction on Pt and aldimine adsorption on the Pt surface suppresses water reduction by blocking a portion of the active sites for H_2 evolution.

When Cu was used, a slight onset shift to the positive direction was observed, indicating that aldimine reduction is more favored than water reduction on Cu (Figure 4.4b). However, cathodic current in the higher overpotential region (V > -1.41 V vs Ag/AgCl, -0.56 V vs. RHE), where both aldimine and water reduction can occur at a considerable rate, was less than the cathodic current observed without HMF. This suggests that in this potential region, aldimine reduction is slower than water reduction and interferes with water reduction. Consequently, reduction of both aldimine and water results in a smaller current than water reduction alone.

When Zn was used, the most dramatic shift in cathodic current onset to the positive direction (by 250 mV) was observed upon the addition of HMF (Figure 4.4c). Also, the cathodic current is significantly higher for all potential region when HMF is present. This shows that Zn is particularly catalytic for reductive amination of HMF.

For the case of Sn and Ag_{sp}, a shift in cathodic onset of 200 mV to the positive direction was observed when HMF was added. Also, a well-defined diffusion-limited reduction peak for aldimine was observed before water reduction, which clearly confirms that HMF reduction is favored over water reduction on the Sn and Ag surface (Figure 4.4d-e). In terms of the onset potential for aldimine reduction, the Ag_{sp} electrode showed the best performance as its onset for HMF reduction occurred at as early as -0.97 V vs. Ag/AgCl (-0.12 V vs RHE).

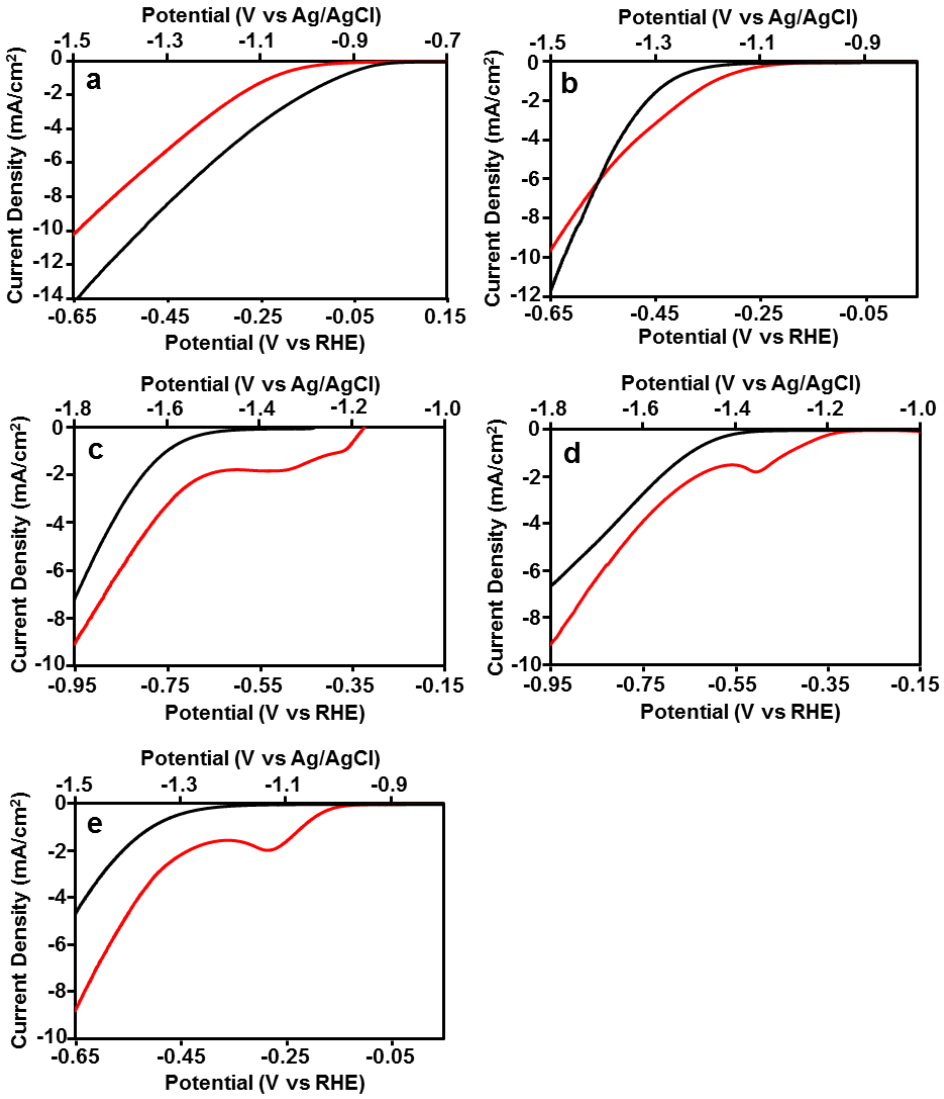

Figure 4.4. LSVs of (a) Pt, (b) Cu, (c) Zn, (d) Sn, and (e) Ag_{sp} electrodes in 0.7 M methylamine buffer solution (pH 11.0) with (red) and without (black) 0.02 M HMF (scan rate 5 mV s^{-1}).

Using the LSVs as a guide for potential regions of interest, reductive amination under constant potential was performed to investigate the effect of potential on amine formation and FE. Results for HMF reductive amination with Ag, Cu, Sn, and Zn can be seen in Table 4.1. The FE and selectivity of each reaction were calculated using equations 1 and 2 found in section

4.2.4. The Pt electrode did not produce any HMF-related reduction products, suggesting that all the cathodic current generated was associated with water reduction. The Cu electrode shows a FE of 84% for aldimine reduction at -1.2 V vs. Ag/AgCl but as the potential becomes more negative, the FE for aldimine reduction gradually decreases as water reduction becomes more favorable.

The Zn, Sn, and Ag_{sp} electrode showed high FE for aldimine reduction in a very wide potential region (-1.3V to -1.6 V vs. Ag/AgCl) because there is a wide window of potential where HMF reduction can occur before water reduction initiates. The most efficient condition for reductive amination in terms of FE was achieved by Zn at -1.4 V vs Ag/AgCl (-0.55 V vs RHE) with 95% FE. In fact, the FE of Zn remained near 90% to E = -1.6 V vs Ag/AgCl (-0.75 V vs RHE), at which point H_2 evolution becomes prevalent according to the LSVs (Figure 4.4e). However, in terms of overpotential required, Zn was not as good as Ag_{sp}. Although the maximum FE achieved by Ag_{sp} was slightly less at 83%, it was achieved at -1.2 V vs. Ag/AgCl where Zn generates negligible current for aldimine reduction.

The selectivity of the aldimine reduction was approximately 100% for most metals and potential conditions. Cu is the notable exception, where both the FE and selectivity decreased when moving to more negative potentials. The products formed were amine dimer and oligomers. For the case of Sn and Zn, the formation of dimer and oligomer of amine was observed only in the low potential region (-1.3 V vs Ag/AgCl). All other potentials yielded HMMAMF exclusively as a conversion product of HMF.

Table 4.1. Results obtained from electrochemical reductive amination of HMF by Cu, Zn, Sn, Ag_{sp}, and Ag_{gd} electrodes at various potentials.[a]

Elec. Mat.	*E* (V) vs Ag/AgCl	Average Current Density (mA/cm^2)	Rate of HMMAMF formation ($\mu mol/cm^2 min$)	FE (%)	Selectivity (%)
Cu	-1.2	9.02	0.789	84	96
	-1.3	14.1	1.04	71	65
	-1.4	34.2	1.38	39	68
	-1.5	46.0	1.22	26	69
Zn	-1.3	9.83	0.831	82	85
	-1.4	21.6	2.14	95	> 99
	-1.5	28.6	2.77	94	> 99
	-1.6	35.9	3.34	90	> 99
Sn	-1.3	7.08	0.515	70	72
	-1.4	21.4	2.08	94	> 99
	-1.5	27.9	2.41	83	> 99
	-1.6	37.0	2.96	77	> 99
Ag	-1.1	6.81	0.558	79	> 99
	-1.2	12.2	1.05	83	> 99
	-1.3	18.8	1.33	68	> 99
	-1.4	41.0	2.17	51	> 99
Ag_{gd}	-1.0	3.86	0.339	85	> 99
	-1.1	18.5	1.91	> 99	> 99
	-1.2	26.7	2.53	91	> 99
	-1.3	33.0	2.83	83	> 99
	-1.4	48.8	2.96	59	> 99

[a] Reported values are averages obtained from three or more measurements. Reaction conditions: 0.7 M methylamine buffer (pH 11.0) containing 0.02 M HMF for 20 C passed.

The ideal catalytic electrode should achieve a high FE for aldimine reduction, like Zn, but require a lower overpotential, like Ag_{sp}. It was demonstrated in chapter 2 that high surface area dendritic Ag electrodes prepared by galvanic displacement of Cu (Figure 4.5a) are particularly catalytic for electrochemical reduction of HMF to BHMF in a pH 9.2 borate buffer solution.[20]

It was postulated that the Ag_{gd} electrode may also be highly catalytic for the reduction of the aldimine form of HMF, achieving the highest FE at the lowest overpotential. While Ag_{gd} is highly catalytic for reduction of HMF of BHMF, since all HMF is present as aldimine in the amine buffer solution (pH 11.0) used in this study, BHMF production cannot compete with reductive amination, ensuring a high FE for aldimine reduction. The LSVs of the Ag_{gd} electrode for water and aldimine reduction is shown in Figure 4.5b in comparison with those of the plain Ag electrode. The current onset for water reduction is -1.2 V vs Ag/AgCl (-0.35 V vs RHE) for both Ag and Ag_{gd}, though the current increases at a greater rate moving to more negative potentials for Ag_{gd}, likely due to the increased surface area. In the presence of HMF, while Ag shows the shift of onset to the positive direction by 200 mV, Ag_{gd} shows the shift of onset by 300 mV, providing a wide window of overpotential where only aldimine can be reduced. The onset shift observed by Ag_{gd} by adding HMF is even greater than that of Zn, which suggests that Ag_{gd} is particularly catalytic for aldimine reduction.

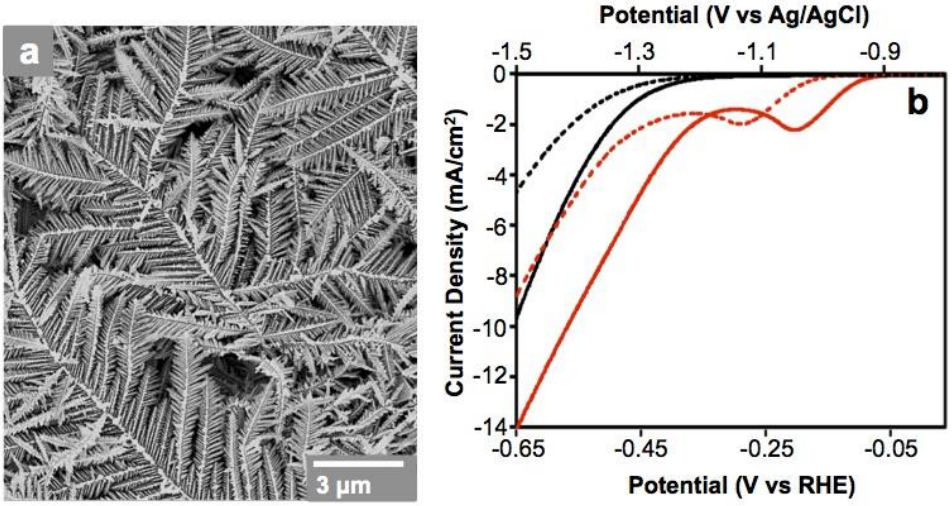

Figure 4.5. (a) SEM of Ag_{gd} electrode and (b) LSVs of Ag_{gd} electrode with (solid) and without (dashed) 0.02 M HMF compared with LSVs of Ag_{sp} electrode (black) with (solid) and without (dashed) 0.02M HMF in a 0.7 M methylamine buffer solution (pH 11.0) (scan rate 5 mV s^{-1}).

The constant potential reduction results show that the FE for reductive amination of HMF on Ag_{gd} is > 99% at -1.1 V vs Ag/AgCl (-0.25 V vs RHE), which is remarkable. The FE for reductive amination decreases for E ≤ -1.2 V vs Ag/AgCl as H_2 evolution initiates. As in the case of Ag, other than H_2, HMMAMF was the only reduction product produced by Ag_{gd}, resulting in the selectivity of >99% for HMMAMF formation.

The surface morphologies of all the electrodes before and after reductive amination are shown in Figure 4.6. No signs of surface changes were observed for the Ag_{sp}, Ag_{gd}, and Sn electrodes. For the Cu and Zn electrodes, minor surface restructuring was observed, which should be due to the interactions with aldimine and not due to dissolution as these metals were cathodically protected during the reduction process.

To further assess the viability of an electrochemical reductive amination, the Ag_{gd} electrode was used to investigate reductive amination of various HMF-based substrates, which included 5-MF, DFF, and FFCA (Figure 4.7a-c). The reductive amination of FFCA results in an artificial amino acid, which could have implications in food and drug applications as well as polymer synthesis.[1,2] The reductive amination product of DFF could also have applications in polymer synthesis.[2]

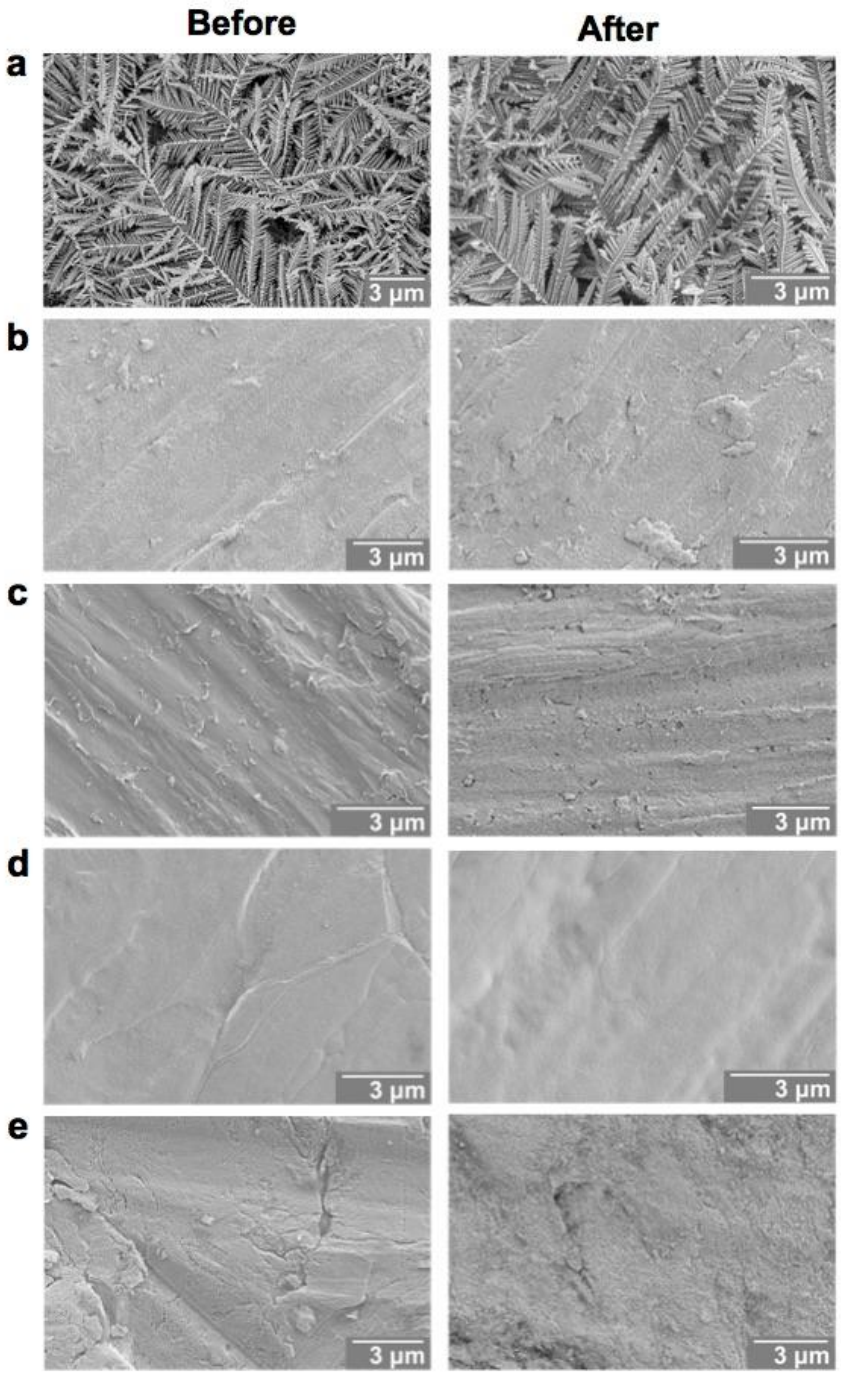

Figure 4.6. SEM images of electrodes before and after passing 20 C for HMF reductive amination. (a) Ag_{gd} (at −1.1 V vs. Ag/AgCl), (b) Ag (at −1.2 V vs. Ag/AgCl), (c) Cu (at -1.2 V vs Ag/AgCl), (d) Sn (at -1.4 V vs Ag/AgCl), and (e) Zn (at -1.4 V vs Ag/AgCl).

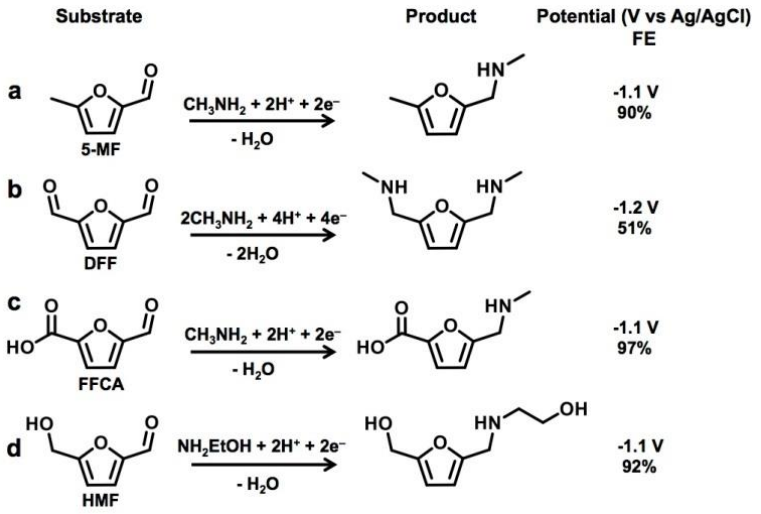

Figure 4.7. Electrochemical reductive amination of (a) 5-MF, (b) DFF, and (c) FFCA with methylamine and (d) HMF with ethanolamine (NH_2EtOH). The potential used for reductive amination and FE for each case is also shown.

The results show that these substrates were efficiently converted to corresponding amines with high FEs (> 90%). The efficiency for the reductive amination of DFF appeared to be low with an observed FE of 51%. However, this is likely due to the low solubility of the resulting diamine, as the product solution became cloudy and a small amount of precipitate could be seen after reductive amination. Judging from the fact that there are no other soluble DFF related reduction products detected by NMR analysis and that water reduction is not efficient at -1.2 V vs. Ag/AgCl, we believe that the actual FE value for the reductive amination of DFF should be much higher than the observed value.

Reductive amination of HMF using ethanolamine instead of methylamine was also tested using a 0.7 M ethanolamine solution containing 20 mM HMF (Figure 4.7d). The use of ethanolamine results in the addition of an alcohol group as well as an amine group, further diversifying the chemistry the product can undergo. The result shows that the reductive amination of HMF with ethanolamine can be achieved with a FE of 92%. LSVs obtained for all

reactions shown in Figure 4.7 can be found in Figure 4.8. It should be noted that addition of 0.02 M HMF to a 0.7 M ammonia solution at pH 11.0 results in very minor aldimine formation, unlike the cases demonstrated when using a primary amine, in which complete conversion of the aldehyde to an aldimine is observed. The equilibrium between aldehyde and aldimine formation with ammonia favors the aldehyde. This is consistent with typical reductive amination with ammonia, which is often conducted in concentrated or liquid ammonia.

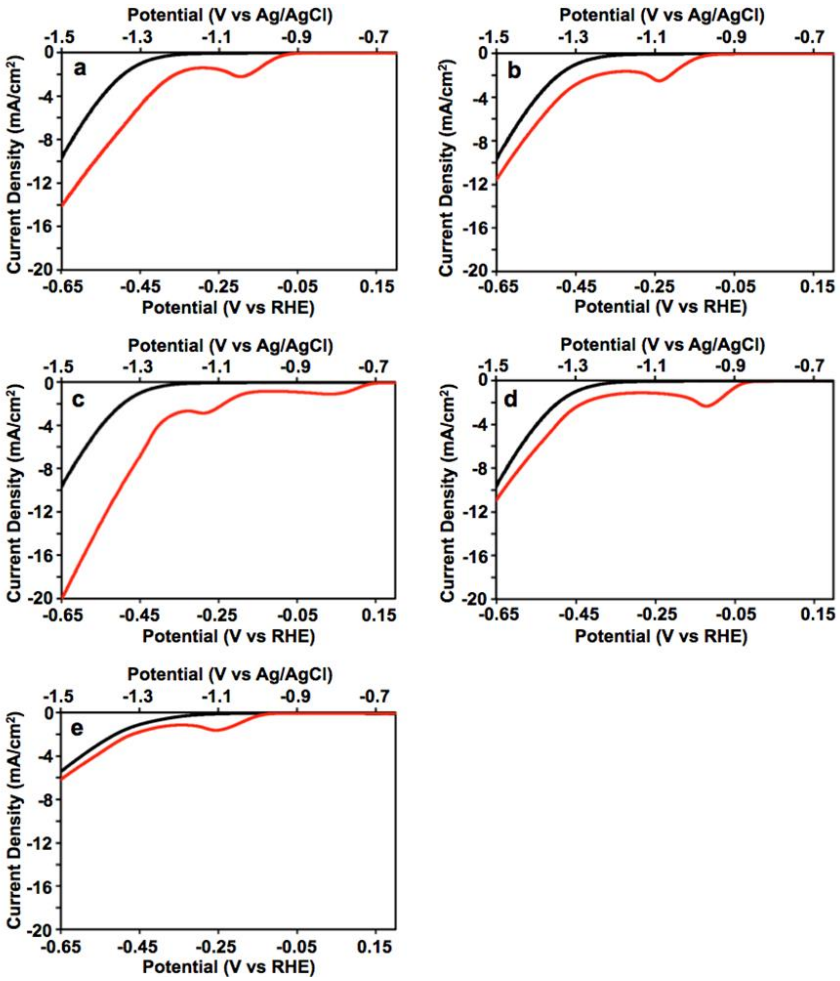

Figure 4.8. (a-d) LSVs of a Ag_{gd} electrode in 0.7 M methylamine buffer solution (pH 11.0) with (red) and without (black) 0.02 M (a) HMF, (b) 5-MF, (c) DFF, (d) FFCA. (e) LSVs of a Ag_{gd} electrode in a 0.7 M ethanolamine solution (pH 11.0) with (red) and without (black) 0.02 M HMF (scan rate 5 mV s^{-1}).

4.4. Conclusion

The successful demonstration of reductive amination using various furfural substrates and primary amines suggests that the electrochemical conditions and catalytic electrodes reported in this study can be used as a general approach for electrochemical reductive amination of biomass intermediates. The Ag_{gd} electrode was identified as an ideal electrode, which achieved the highest FE and selectivity with a minimum overpotential necessary. The conditions and electrodes reported in this study may also be used for many of the compounds that have been reductively aminated via traditional routes. The use of water as the hydrogen source at ambient temperatures without requiring chemical reducing agents will decrease the cost and environmental concerns associated with conventional reductive amination.

4.5. References

1. J. P. Klein, *International Patent Application*, PCT/US2014/022798, 2014.
2. A. Gandini, *Polym. Chem.*, 2010, **1**, 245-251.
3. A. Feriani, G. Gaviraghi, G. Toson, M. Mor, A. Barbieri, E. Grana, C. Boselli, M. Guarneri, D. Simoni and S. Manfredini, *J. Med. Chem.*, 1994, **37**, 4278-4287.
4. B. Plitta, E. Adamska, M. Giel-Pietraszuk, A. Fedoruk-Wyszomirska, M. Naskret-Barciszewska, T. Markiewicz, Wojciech and J. Barciszewski, *Eur. J. Med. Chem.*, 2012, **55**, 243-254.
5. Z. Xu, P. Yan, W. Zy, S. Jia, Z. Xia, B. Chung and Z. C. Zhang, *RSC Adv.*, 2014, **4**, 59083-59087.
6. A. Cukalovic and C. V. Stevens, *Green Chem.*, 2010, **12**, 1201-1206.
7. G. Chieffi, M. Braun and D. Esposito, *ChemSusChem*, 2015, **8**, 3590-3594.
8. M. Chatterjee, T. Ishizaka and H. Kawanami, *Green Chem.*, 2016, **18**, 487-496.
9. T. Xiang, X. Liu, P. Yi, M. Guo, Y. Chen, C. Wesdemiotis, J. Xu and Y. Pang, *Polym. Int.*, 2013, **62**, 1517-1523.
10. J. D. Garber and R. A. Gasser, *US Pat.*, 2995582, 1961.
11. A. Simion, C. Simion, T. Kanda, S. Nagashimi, Y. Mitoma, T. Yamada, K. Mimura and M. Tashiro, *J. Chem. Soc., Perkin Trans. 1*, 2001, 2071-2078.
12. T. Tsukinoki, Y. Mitoma, S. Nagashima, T. Kawaji, I. Hashimoto and M. Tashiro, *Tetrahedron Lett.*, 1998, **39**, 8873-8876.
13. Y. D. Smirnov and A. P. Tomilov, *Zh. Org. Khim+.*, 1992, **28**, 51-58.
14. G. B. Giovenzana, D. Imperio, A. Penoni and G. Palmisano, *Beilstein J. Org. Chem.*, 2011, **7**, 1095-1099.

15. ed. P. Knochel and G. A. Molander, *Comprehensive Organic Synthesis, Volume 8: Reduction (2nd Edition)*, Elsevier, Amsterdam, 2014.

16. J. J. Martinez, E. Nope, H. Rojas, M. H. Brijaldo, F. Passos, and G. Romanelli, *J. Mol. Catal. A*, 2014, **392**, 235-240.

17. A. F. Abdel-Magid, K. G. Carson, B. D. Harris, C. A. Maryanoff and R. D. Shah, *J. Org. Chem.*, 1996, **61**, 3849-3862.

18. T. Pienemann, H. –J. Schäfer, *Synthesis*, 1987, **11**, 1005-1007.

19. R. J. Cvetovich, J. S. Amato, L. DiMichele, L. Weinstock and G. Hazen, *J. Org Chem.*, 1997, **62**, 6697-6698.

20. H. Lund, *Acta Chem. Scand.*, 1959, **13**, 249-267.

21. V. Concialini, S. Roffia and D. Savoia, *Gazz. Chim. Ital.*, 1195, **125**, 77-81.

Chapter 5. Electrochemical Synthesis and Application of Metal-Polymer Heterogeneous Catalysts for CO_2 Reduction

5.1. Introduction

5.1.1. Electrochemical Reduction of CO_2

Dependence on fossil fuels since the start of the industrial revolution has led to significant increases in atmospheric CO_2 levels and a number of environmental concerns.[1-4] Several methods of carbon capture and sequestration, fixation, and transformation have been proposed and studied to remove excess CO_2 from the atmosphere.[1-5] While removing excess CO_2 from the atmosphere will alleviate concerns of environmental impact, transformation of CO_2 to a useful product, such as a liquid fuel, is a more promising approach as it may also decrease dependence on fossil fuels. Therefore, developing an efficient and practical route to accomplish those transformations is of great interest.

It has long been known that CO_2 can be electrochemically reduced at metal electrodes such as copper and tin.[4,6,7] However, advancement and implementation of electrochemical CO_2 reduction has been delayed due to the need of a significant overpotential (~1 V) and the complexity of CO_2 reduction, often resulting in numerous products in an unselective manner.[4-8] Common reduction reactions observed in aqueous solutions saturated with CO_2 are shown in Equations 5.1-5.6. Reduction potentials are vs. Ag/AgCl at pH 7, 25 °C, 1 atm gas pressure

$$CO_2 + 2H^+ + 2e^- \leftrightarrow CO + H_2O \qquad E° = -0.73 \qquad (5.1)$$

$$CO_2 + 2H^+ + 2e^- \leftrightarrow HCO_2H \qquad E° = -0.81 \qquad (5.2)$$

$$CO_2 + 4H^+ + 4e^- \leftrightarrow HCHO + H_2O \qquad E° = -0.68 \qquad (5.3)$$

$$CO_2 + 6H^+ + 6e^- \leftrightarrow CH_3OH + H_2O \qquad E° = -0.58 \qquad (5.4)$$

$$CO_2 + 8H^+ + 8e^- \leftrightarrow CH_4 + 2H_2O \qquad E° = -0.44 \qquad (5.5)$$

$$2H^+ + 2e^- \leftrightarrow H_2 \qquad E° = -0.61 \qquad (5.6)$$

The product distribution varies with a number of factors including applied potential, electrode material, electrolyte, solvent, pH, CO_2 pressure, and temperature.[6-11] Variations in the applied potential alone (while keeping all other variables constant) is enough to cause drastic changes to the products observed. Kuhl *et al*. observed 16 products on a Cu electrode just with changes to the applied potential.[9] As a result of numerous products being generated, the efficiency and selectivity for any single product is often low. Therefore, development of electrode materials which are highly catalytic and selective toward CO_2 reduction is of great interest.

Similar to the enhancement that was discussed in chapters 2 and 4 for electrochemical reduction and reductive amination of HMF on high surface area Ag films compared to flat Ag films, it has been demonstrated that the morphology of the electrode surface can alter the catalytic ability of a material for electrochemical CO_2 reduction.[7,12] Furthermore, it has been postulated that fine tuning of compositions (alloying), particle size, and interfacial atomic arrangements of Cu and Sn can significantly enhance the selectivity and efficiency of CO_2 reduction compared to simple forms of metal foils employed in previous studies.[13] However, almost no research has been conducted toward this direction due to the lack of synthesis ability to systematically tune these features. The work discussed herein is the utilization of compositionally and morphologically versatile electrochemical synthesis to produce high surface area Cu and Sn electrodes with systematically altering compositions and morphologies to identify optimum catalytic structures while enhancing the general understanding of CO_2 reduction.

5.1.2. High surface area metal-coated nanosphere polypyrrole films

It has recently been demonstrated that high surface area nanosphere polypyrrole electrodes can be prepared under cathodic deposition conditions.[14,15] This method is based on in situ cathodic generation of an oxidizing agent, NO^+, which can oxidatively polymerize monomers into conducting polymers at the cathodic surface.[14,15] This new polymerization method makes it possible to assemble metal-conducting polymer hybrid films via one-step cathodic deposition, which is not possible by conventional anodic polymerization. This synthesis method was exploited to generate a variety of Cu-, Sn-, and Cu-Sn-metal alloy nanoparticles/polypyrrole (PPy) composite electrodes, hereafter designated as Cu-PPy, Sn-PPy, and Cu-Sn-PPy, respectively. The resulting films had high surface areas and an increased number of sites for CO_2 reduction compared to metal foils and lower surface area films. Moreover, this method permitted an easy and systematic tuning of alloy compositions by simply changing the solution metal ion compositions, which would allow a remarkable freedom in studying the effect of metal compositions on the efficiency and selectivity of CO_2 reduction. A limited few previous studies have demonstrated how a subtle change in catalyst composition can drastically affect the product composition resulting from CO_2 reduction, which supports the importance of this work that examined the composition effect.[13]

5.2. Experimental

5.2.1. Materials

Copper (II) nitrate, trihydrate (99%) was purchased from Acros Organics. Copper (II) chloride, dihydrate (99+%), potassium hydrogen carbonate (99.7% -110.5%, dried basis), silver nitrate (99.9+%), tin foil (0.025 mm thick, 99.9%), and tin (II) sulfate (≥ 95.5%) were purchased

from Alfa Aesar. Copper foil (1 Mil, 0.001 in. thick, 99.9%) was purchased from Nimrod Hall Copper Foil Company. Nitric acid (70%), pyrrole (98%), sodium nitrate (≥ 99%), and tin (II) chloride, dihydrate (98%) were purchased from Sigma Aldrich. Carbon dioxide gas (99.999%), helium gas, ultra-high purity (99.999%), hydrogen gas standards (500 ppm and 2000 ppm in nitrogen gas) and hydrocarbon gas standard (500 ppm carbon monoxide, 500 ppm methane, 500 ppm ethane, 500 ppm ethene, and 500 ppm ethyne in nitrogen gas) were purchased from Airgas. Graphite rods (99.995%) were purchased from Sigma Aldrich.

5.2.2. Preparation of Electrodes

The Cu and Sn electrodes used in this study were prepared by cutting the foil to pieces with dimensions of 1.5 cm x 2.5 cm. The Cu and Sn surfaces were first rinsed with 2-propanol and water, then cleaned by immersing in 1 M HCl for 1 minute to remove surface oxides. After rinsing with DI water and drying, Cu tape was attached to the foil electrodes to enable connection to the potentiostat lead. The backside and top 0.5 cm of the Cu or Sn foil electrodes were then covered with Teflon tape to yield a 3.0 cm^2 working area. The cleaning and preparation of electrodes were performed immediately before use in experiments. The Pt counter electrodes were prepared by sputter coating a 100 nm platinum layer over a 20 nm titanium layer onto cleaned glass slides. The dimension of the working area of the Pt counter electrode was 2.0 cm x 2.0 cm.

To prepare the metal-PPy films, a deposition solution consisting of 0.5 M $NaNO_3$, 0.4 M HNO_3, and the desired concentration of $Cu(NO_3)_2$ or $SnCl_2$ was prepared and heated to 45 °C. To minimize bulk polymerization of pyrrole in the solution, 0.2 M pyrrole was added just prior to deposition. An undivided three-electrode cell was used for depositions with Cu foil as the working electrode, Pt as the counter electrode, and Ag/AgCl (4M KCl) as the reference

electrode. The codeposition of polypyrrole and copper or tin metals was performed at -0.65 V for 50 C passed. A Princeton Applied Research VMP2 multichannel potentiostat was used for electrodeposition and CO_2 reduction studies. Prior to use for CO_2 reduction experiments, the edges of the film were covered and sealed with nail polish in order to prevent solution from seeping under the Teflon tape during electrolysis.

5.2.3. Solution Preparation

Electrochemical CO_2 reduction experiments were conducted in a 0.1 M $KHCO_3$ solution saturated with CO_2 (pH 6.8). To prepare the solution, CO_2 gas was bubbled through a 0.1 M $KHCO_3$ solution using a gas disperser (glass tube with porous glass frit attached to the end to decrease gas bubble size and increase dispersion of the gas in the solution). To ensure maximum CO_2 saturation, the solution was sparged with CO_2 for at least one hour. The solution was then introduced to the working cell (divided or undivided) and sparged for another 5 minutes to ensure maximum CO_2 saturation in the solution and the headspace. Sparging was continued until immediately preceding electrolysis experiments, and gas flow in the headspace was continued for unsealed, undivided cell experiments in an attempt to maintain high CO_2 saturation and to keep the headspace and solution free from O_2 from air.

5.2.4. Characterization

The as-deposited electrodes were analyzed by X-ray diffraction (XRD) using a Scintag X2 diffractometer (Cu Kα radiation) to confirm the crystallinity of the films and to identify potential alloys. Field Emission Scanning Electron Microscopy (SEM) and energy-dispersive X-ray spectroscopy (EDX) were conducted on a FEI Nova nanoSEM with through-the-lens high resolution detector and equipped with an Oxford INCA 250 EDX system at accelerative voltages of 5-20 kV to observe morphologies and elemental compositions of the as-deposited films. The

SEM samples were first sputter coated with approximately 2 nm thick Pt to ensure conductivity of the samples and to prevent charging while collecting images. Charging can lead to heat buildup and subsequent distortion and destruction of the PPy. CO_2 reduction products were detected on a SRI 8610C Gas Chromatograph Multiple Gas #3 with He carrier gas, HayeSep D and MoleSieve 13X columns, helium ionization detector (HID) and thermal conductivity detector (TCD). A hydrocarbon gas standard was used to determine the concentration of the products.

5.2.5. Electrochemical Reduction of CO_2

The catalytic ability of the electrodes was first examined by performing linear sweep voltammetry (LSV) in an undivided three-electrode cell in 0.1 M $KHCO_3$ solutions sparged with either Ar to removed dissolved O_2, or saturated with CO_2. Addition of CO_2 to the 0.1 M $KHCO_3$ solution resulted in a decrease in the pH to 6.8n. A small amount of concentrated sulfuric acid was added to the 0.1 M $KHCO_3$ sparged with Ar to ensure the pH of the solutions with and without CO_2 were the same, thus enabling proper comparison of reduction onsets. Graphite rods were used as the counter electrodes in both LSV and constant potential electrolysis experiments. The main competing reaction of CO_2 reduction is water reduction, and large overpotentials (>1 V) are often required for electrochemical CO_2 reduction. When Pt is used as the anode, some of it may oxidize, dissolve into the solution, and redeposit at the cathode, further improving the water reduction abilities of the material and thereby decreasing the efficiency of CO_2 reduction. Graphite rods were used to prevent this possibility. The LSVs were performed by sweeping the potential toward more negative potentials from the open circuit potential at 5 mV/s. An increase in current for an LSV with CO_2 compared to without can be attributed to CO_2 reduction.

To determine potential dependence on CO_2 reduction, constant-potential electrolysis was performed in a sealed, divided three-electrode cell. The initial cell design was a small H-shape split cell with glass frit and Teflon caps to seal the cell, affording 14.0 mL for the headspace. A second cell was designed that afforded more secure seals and a much larger headspace for product accumulation. The solution was sparged and introduced to the split cell as previously described. The working and counter electrodes were attached to copper rods. Teflon tape was used to cover any exposed copper of the copper rods within the cell, with the rods being fitted through an o-ring to create an air-tight seal. The tops of the copper rods, which were protruding from the cell, were connected to the potentiostat leads.

To decrease resistance across the frit, the diameter of the glass frit was increased from 1 cm in the small cell to 3 cm in the large cell. The Ag/AgCl reference electrode was introduced to the cell through a special port equipped with an o-ring to hold the electrode in place and create an air-tight seal. Gas sampling was performed through another port on the cell equipped with a septum. The sealed cell afforded a 95.0 mL headspace. 0.5 mL gas samples of the headspace were taken with an airtight syringe just prior to electrolysis, after 30 minutes, and after 60 minutes of electrolysis. The potentials analyzed were from -1.0 V to -1.75 V vs Ag/AgCl at 250 mV increments. Liquid products were not analyzed. FE was calculated using Equation 5.7, where F is the Faraday constant (96485 C/mol) and n is the number of electrons required for the conversion of CO_2 to CO, CH_4, or C_2H_4 , which is 2,8, and 12, respectively.

$$\text{FE}\ (\%) = \frac{\text{mol of product}}{\text{Total charge passed (C)}/\ (\text{F}\times\text{n})} \times 100\% \qquad (5.7)$$

5.3. Results and Discussion

5.3.1. Metal-PPy Codepositon Films

The initial method developed for cathodic deposition of PPy called for the use of a sacrificial Cu counter electrode.[14] The Cu served to improve conductivity of the film, since PPy is insulating at the potential range for deposition, and also acted as an adhesion layer between PPy particles. Consequently, the metal content remained fairly low at 2-3% by EDX analysis. The PPy particles deposited in this manner are 500 nm to 1 μm in diameter (Figure 5.1). The deposition of smaller particles would lead to greater surface area, thereby increasing the current density and number of active sites for CO_2 reduction.

In order to have more control over the metal content, particle size, morphology, and surface roughness of the PPy films, metal salts (0. 2 M to 0.02 M) were added to the deposition solution. In this manner Cu-PPy, Sn-PPy and Cu-Sn-PPy films were deposited with varying morphologies and metal contents. A decrease in particle size and an increase in surface roughness is observed with an increase in the concentration of the metals in the solution. This arises from the core-shell nature of the films. As the PPy particles deposit, the higher concentration of metal in the solution leads to capping of the PPy core with a metal shell. Further particle growth is less preferential to new particle growth. Thus, the films are often an agglomeration of increasingly smaller spherical particles. The Cu-PPy films were composed of smaller and rougher particles than the PPy films deposited with a Cu counter, with particle sizes in the range of 50-250 nm for films made with 0.2 M $Cu(NO_3)_2$ in the deposition solution (Figure 5.2a). As the Cu^{2+} concentration in the deposition solution decreased, a slight increase in particle size and decrease in surface roughness was observed (Figure 5.2b). XRD analysis did

not yield any new peaks since the Cu-PPy films were deposited on a Cu substrate. Any Cu peaks from the deposited film would appear at the same angles as the substrate and thus be obscured.

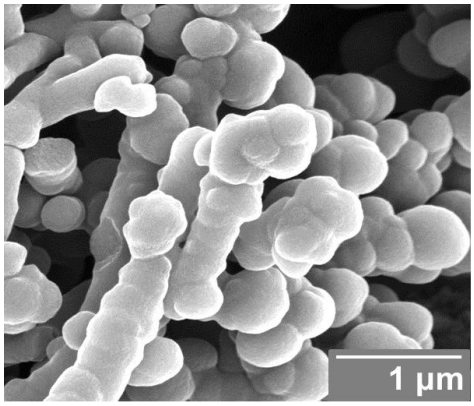

Figure 5.1. SEM image of a PPy film deposited for 50 C at -0.65 V vs Ag/AgCl using a sacrificial copper counter electrode. (Deposition solution: 0.4 M HNO_3, 0.5 M $NaNO_3$, 0.2 M pyrrole, pH 0.4, 45 °C)

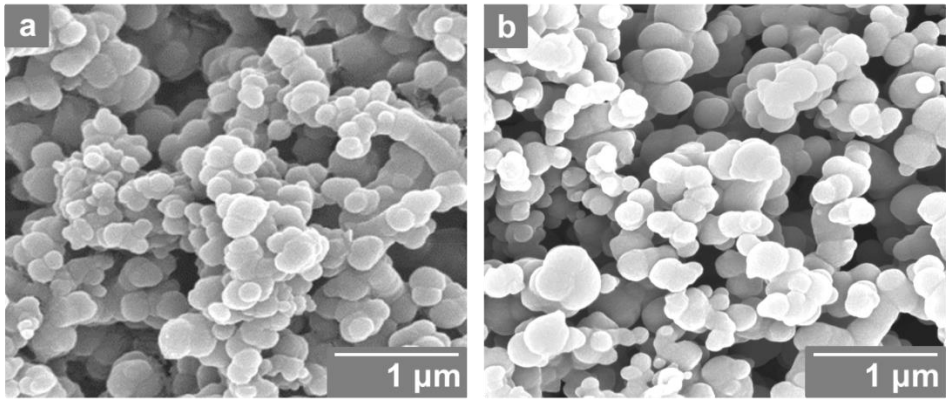

Figure 5.2. SEM images of Cu-PPy films deposited for 50 C at -0.65 V vs Ag/AgCl by the addition of (a) 0.2 M $Cu(NO_3)_2$ and (b) 0.05 M $Cu(NO_3)_2$ to the PPy deposition solution (0.4 M HNO_3, 0.5 M $NaNO_3$, 0.2 M pyrrole, pH 0.4, 45 °C).

The changes in particle size are more apparent and drastic for Sn-PPy films (Figure 5.3), with particles ranging from <50 nm for films deposited from a solution containing 0.2 M $SnCl_2$ (Figure 5.3a) to 200-500 nm for films deposited from a solution containing 0.02 M $SnCl_2$ (Figure 5.3d). The particles deposited under the former conditions are sufficiently small enough to cause a great increase in the surface area, but the particles have deposited closely enough so as to largely eliminate the porosity of the film, decreasing the effective surface area. Sn-PPy films deposited from a solution containing 0.1 M $SnCl_2$ retained the porous nature of the PPy films and had sufficiently small particles so as to greatly increase the effective surface area compared to standard PPy films. All Sn-PPy particles were observed to possess a greater surface roughness than PPy particles alone, further increasing the effective surface area. The presence of Sn in the films was confirmed by EDX and XRD. The nanoparticulate nature of the Sn in the films results in only a single, broad and weak (200) peak (Figure 5.4). Peaks generated by the Cu substrate are denoted by *.

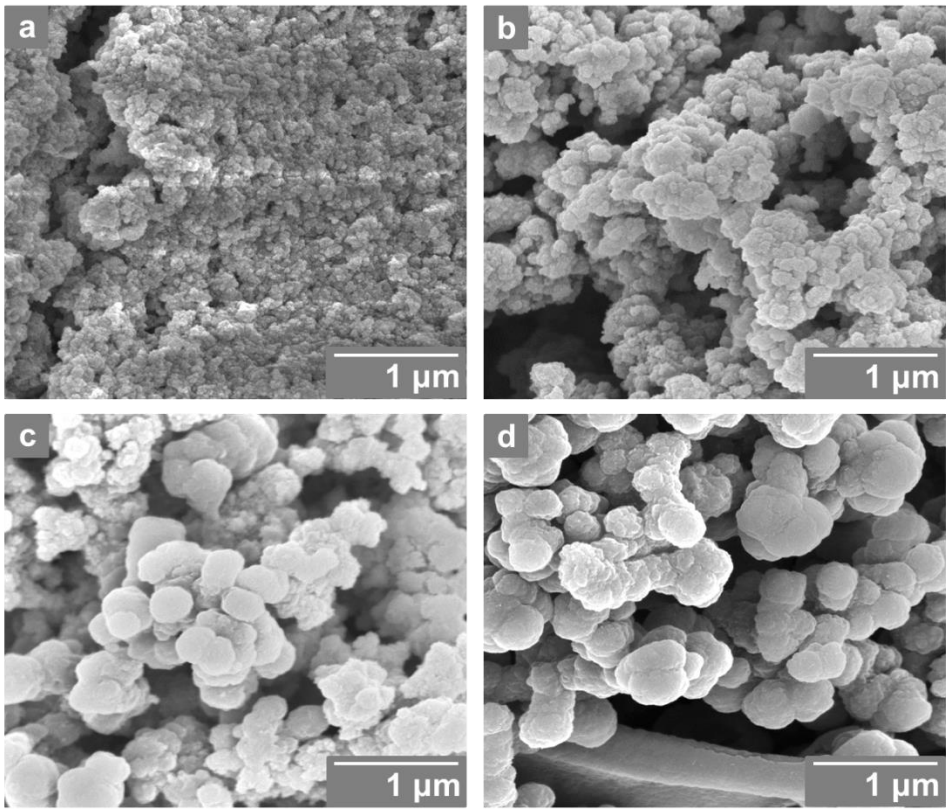

Figure 5.3. SEM images of Sn-PPy films deposited for 50 C at -0.65 V vs Ag/AgCl by the addition of (a) 0.2 M $SnCl_2$, (b) 0.1 M $SnCl_2$, (c) 0.05 M $SnCl_2$, and (d) 0.02 M $SnCl_2$ to the PPy deposition solution (0.4 M HNO_3, 0.5 M $NaNO_3$, 0.2 M pyrrole, pH 0.4, 45 °C).

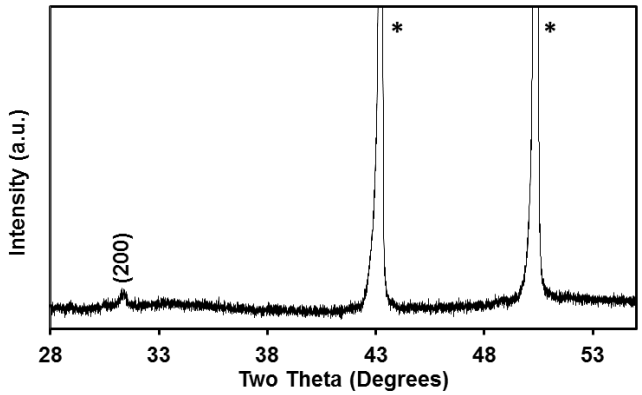

Figure 5.4. XRD pattern of an as-deposited Sn-PPy film deposited for 50 C at -0.65 V vs Ag/AgCl by the addition of 0.1 M $SnCl_2$ to the PPy deposition solution (0.4 M HNO_3, 0.5 M $NaNO_3$, 0.2 M pyrrole, pH 0.4, 45 °C). Peaks generated by the Cu substrate are denoted by *.

While Cu and Sn have distinctive properties and performances for electrochemical CO_2 reduction, a composite film of the two may result in synergistic properties (e.g. reduction of CO_2 to CO on Sn followed by reduction of CO to other species on Cu), or may behave entirely differently than the two. To deposit Cu-Sn films, various concentrations of $Cu(NO_3)_2$ and $SnCl_2$ were added to the PPy deposition solution. A chemical reaction occurred between Sn and Cu species in the solution, however, resulting in what appeared to be reduction of Cu^{2+} to Cu^{1+} and oxidation of Sn^{2+} to Sn^{4+} and precipitation of SnO_2, as evidenced by the solution turning green with a white precipitate forming at the bottom of the beaker. To minimize this reaction, $SnCl_2$, which dissolved slowly, was added to the solution containing HNO_3 and $NaNO_3$ at 45 °C and stirred until fully dissolved. Then, immediately prior to deposition $Cu(NO_3)_2$ and pyrrole, which dissolve readily, were added to the solution.

The films deposited in this manner tended to be copper-rich. Films deposited from a solution of equal concentrations of Cu^{2+} and Sn^{2+} consistently deposited three times as much Cu than Sn as determined by EDX. All films deposited from a solution containing an excess of Cu^{2+} relative to Sn^{2+} resulted in the deposition of Cu cubes, as shown in Figure 5.5a, with an even greater ratio of Cu-to-Sn deposited (e.g. a solution containing 0.2 M Cu^{2+} and 0.02 M Sn^{2+} deposited films containing 15 times as much Cu than Sn). Of all the Sn-PPy films deposited, those deposited from a solution containing 0.1 M Sn^{2+} contained the most desirable morphology. Therefore, Cu-Sn-PPy films were deposited from solutions containing 0.1 M Sn^{2+} and varying concentrations of Cu^{2+} in order to observe changes in morphology and metal content. The resulting films, shown in Figure 5.5, primarily possess the surface roughness and particle size of the Sn-PPy films but with 3D structure varying from porous raised pillars to flat films for a corresponding decrease of Cu^{2+} in the solution from 0.1 M to 0.02 M.

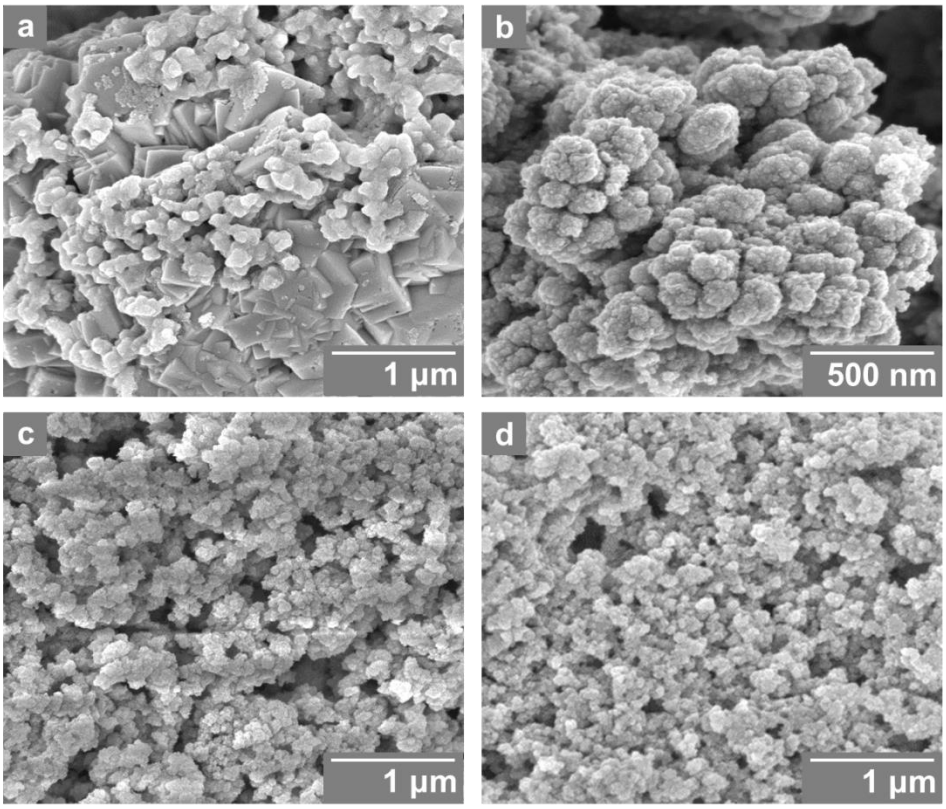

Figure 5.5. SEM images of Cu-Sn-PPy films deposited for 50 C at -0.65 V vs Ag/AgCl by the addition of 0.1 M $SnCl_2$ and (a) 0.2 M $Cu(NO_3)_2$, (b) 0.1 M $Cu(NO_3)_2$, (c) 0.05 M $Cu(NO_3)_2$, or (d) 0.02 M $Cu(NO_3)_2$ to the PPy deposition solution (0.4 M HNO_3, 0.5 M $NaNO_3$, 0.2 M pyrrole, pH 0.4, 45 °C).

Cu-Sn-PPy films deposited from a solution containing 0.1 M of both Cu^{2+} and Sn^{2+} possessed the most interesting and promising morphology and surface area for CO_2 reduction. The films were composed of aggregates of 20-50 nm particles, greatly increasing the surface area compared to the other Cu-Sn-PPy films. As previously mentioned, the Cu-to-Sn content of the films was 3:1. XRD analysis revealed that the film deposited as an alloy as opposed to separate layers or particles of Cu and Sn. The exact composition and crystal structure is unknown since there are many CuSn alloys, many with very similar diffraction patterns to those observed for the Cu-Sn-PPy film. No Sn peaks can be observed, and the excess copper, if any, likely deposited as

Cu metal, the peaks of which would be obscured by the peaks for the Cu substrate that appear at the same angles as was the case for the Cu-PPy films. Figure 5.6 demonstrates the XRD pattern of the Cu-Sn-PPy film with peaks for the Cu-Sn alloy denoted by a red circle and Cu substrate peaks denoted by *.

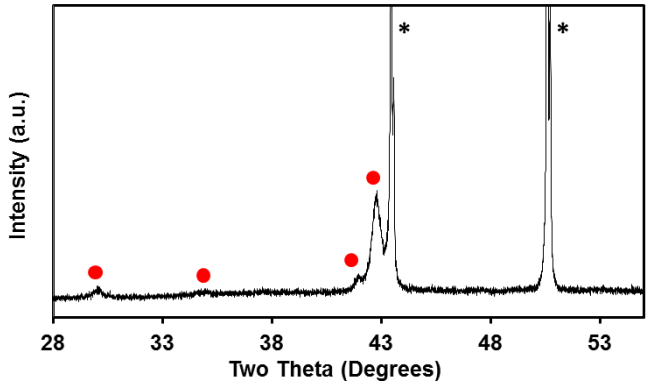

Figure 5.6. XRD pattern of an as-deposited Cu-Sn-PPy film deposited for 50 C at -0.65 V vs Ag/AgCl by the addition of 0.1 M $Cu(NO_3)_2$ and 0.1 M $SnCl_2$ to the PPy deposition solution (0.4 M HNO_3, 0.5 M $NaNO_3$, 0.2 M pyrrole, pH 0.4, 45 °C). Peaks generated by the Cu-Sn alloy are denoted by a red circle; peaks generated Cu substrate are denoted by *.

5.3.2. CO_2 Reduction: Linear Sweep Voltammetry

The Cu-PPy, Sn-PPy, and Cu-Sn-PPy films that were deposited were analyzed for their CO_2 reduction ability by performing LSVs in a 0.1 M $KHCO_3$ solution with and without CO_2 saturation. In conducting the LSVs, the current observed for a solution without CO_2 can be attributed to water reduction to H_2. Therefore, an earlier cathodic current onset for a solution with CO_2 saturation than without indicates CO_2 reduction is occurring. The LSV scans were conducted only once each for without and with CO_2 saturation, first in a solution sparged with Ar, then in a CO_2 saturated solution. A reduction wave was present in the scans without CO_2

that was not present in the scan with CO_2 (Figure 5.7). This is likely due to reduction of metal oxides which could have formed on the surface of the films upon exposure to air, as evidenced by the reduction wave appearing at different potentials for a Cu-PPy and Sn-PPy film, as shown in Figures 5.7a and 5.7b. The exceptions to this trend are for Cu-Sn-PPy films, in which reduction waves are present for with and without CO_2. A decrease in the peak current observed with decreasing Cu and Sn content of the films (Figures 5.7c and 5.7d) indicates that this feature may simply be a result of incomplete reduction of the film during the first LSV scan. Repeated scans in the solution without CO_2 would have clarified this and made LSV comparisons for all metal-PPy films more useful.

All films examined showed a slight early reduction onset for CO_2 saturated solutions, but the current increased at a slower rate than for without CO_2 (water reduction), resulting in the same or greater current at more negative potentials for water reduction than for CO_2 reduction. This suggests that CO_2 reduction is occurring on the films, and the cause for decreased current at more negative potentials may be due to kinetically slower reduction of CO_2 compared to water reduction. Cu-PPy films achieved much greater currents and had earlier current onsets than for Sn-PPy films, as shown in Figures 5.7a and 5.7b. The reduction onset for a Cu-PPy film appears as early as -0.8 V vs Ag/AgCl in a 0.1 M $KHCO_3$ solution saturated with CO_2 (pH 6.8), while the reduction onset for a Sn-PPy films in the same solution does not appear until approximately -1.05 V vs Ag/AgCl. Reduction onsets for Cu-Sn-PPy films in the same solution are obscured by the reduction wave as discussed. The reduction onset and overall current observed for Cu-PPy may be better than Sn-PPy as a result of improved CO_2 reduction performance on Cu, or as a result of better water reduction capability of Cu than Sn. The effective working surface area of the Cu-PPy and Sn-PPy films is unknown, but the Sn-PPy films appear to have smaller particle

sizes and greater overall surface area, which would exclude surface area arguments as a reason for increased current on Cu-PPy.

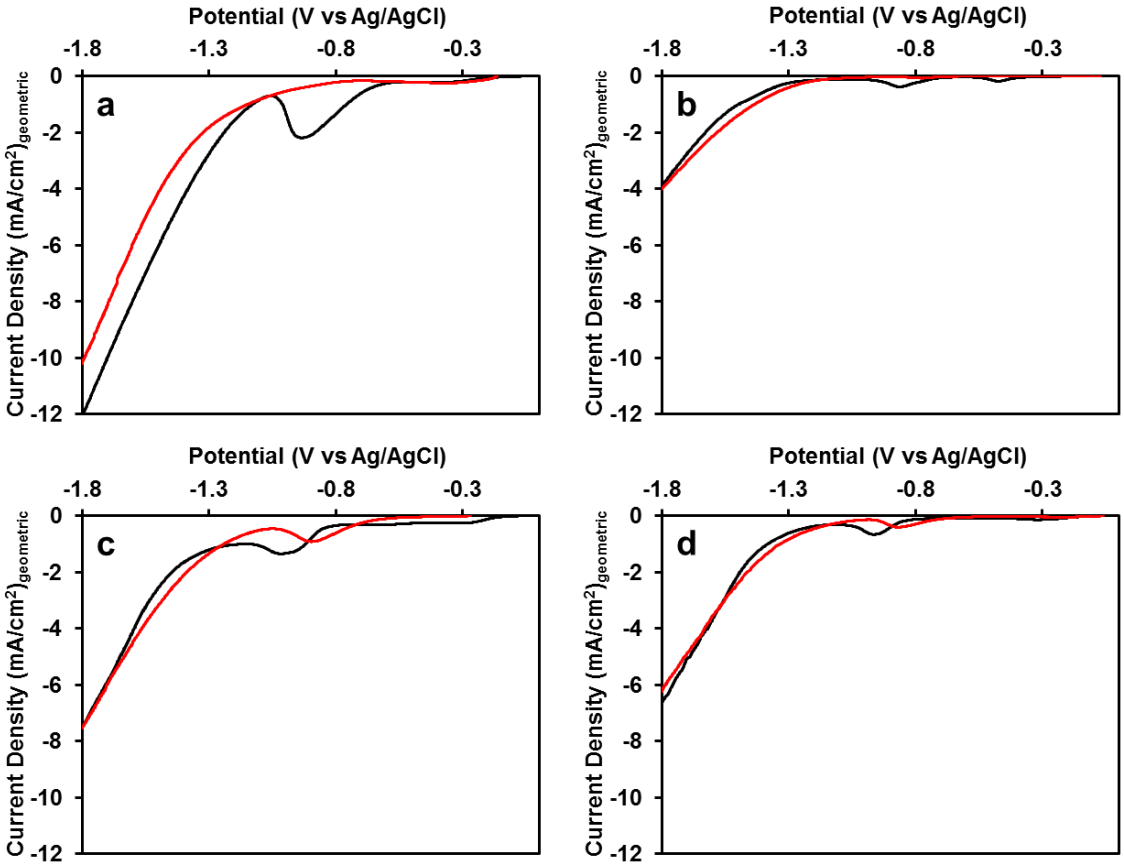

Figure 5.7. LSVs of (a) 0.1 M Cu-PPy, (b) 0.1 M Sn-PPy, (c) 0.05 M Cu-, 0.05 M Sn-PPy, and (d) 0.02 M Cu-, 0.02 M Sn-PPy electrodes in 0.1 M $KHCO_3$ (pH 6.8) sparged with CO_2 gas (red) or with Ar gas (black) (scan rate: 5 mV/s). The effective surface area of the films is unknown, therefore current density has been normalized to the geometric area of the films, 3 cm^2.

5.3.3. CO_2 Reduction: Constant-Potential Electrolysis

Constant-potential electrolysis was performed to further analyze the CO_2 reduction ability of the films and to determine potential-dependent product formation. This was conducted in one of two cells as previously described. Cu-PPy, Sn-PPy, and Cu-Sn-PPy films were analyzed over a range of potentials (-1.0 V to -1.75 V vs Ag/AgCl) and compared to Cu and Sn foil electrodes. The results from the first small split cell (Table 5.1) demonstrate that CO_2 reduction is occurring, and particularly on Sn-PPy films much more efficiently than other foil or PPy based electrodes, achieving 11.4% FE for CO production at -1.5 V vs Ag/AgCl. The metal-PPy films had higher charge passed, and thus higher current density than the metal foil counterparts for the same potentials and time durations. Furthermore, the formation rate and FE for reduction of CO_2 to CO is much greater on the metal-PPy films than the corresponding metal foils at the same potentials. This may be an indication that the effective surface area of the metal-PPy films was greater than that of the metal foils. Increased surface area alone would not account for an increase in FE, however. The results do indicate that the morphology and orientation of the Cu-PPy and Sn-PPy films led to more active sites for CO_2 reduction relative to the surface area of the films than for the foil electrodes.

The ability of Sn to break C-O bonds and reduce CO_2 to CO or other further reduced species has been called into question.[1,3,6] These results clearly indicate the ability of Sn-PPy films to perform this reduction. In fact, CO_2 reduction proceeded to a much greater extent on Sn-based electrodes than for Cu-based electrodes, where CH_4 production was observed but with efficiencies well below 0.5%. The main reduction product for Cu-based films was H_2. This further supports the notion that enhanced current was observed for Cu-PPy films due to better water reduction capabilities of Cu than Sn. Overall performance for CO_2 reduction was low for

all materials and conditions tested. One reason for this is that during electrolysis the pressure would increase rapidly, often resulting in the Teflon cap being pushed off, thereby losing the seal and an unknown quantity of product. Alternatively, if the seal of cell caps was maintained, some of the solution would get pushed to the other side of the cell through the frit, causing a change in the headspace. Additionally, the small headspace led to quick accumulation of product, which was often too concentrated for the upper detection limit of the GC HID detector, as was the case for nearly every trial for H_2 detection and for a the 60 minute measurements of Sn- and Cu-Sn-PPy films. Therefore, production of CO may have actually surpassed 11.4 % FE for the Sn-PPy film at -1.5V vs Ag/AgCl after 60 minutes of electrolysis.

The small frit of the cell resulted in high resistance between the working and counter electrodes, causing the potential at the counter electrode to drift to extreme potentials (>10 V vs Ag/AgCl) in order to match the current of the working electrode. The potential at the working electrode was limited to -1.5 V vs Ag/AgCl since anything greater resulted in potentials at the counter electrode that were too extreme and could not be achieved by the potentiostat in order to match the current.

Table 5.1. Results of electrochemical reduction of CO_2 in 0.1 M $KHCO_3$ (pH 6.8) at Cu, Cu-PPy, Sn, Sn-PPy, and Cu-Sn-PPy electrodes in a small split cell.

Electrode Material[a]	Potential (V vs Ag/AgCl)	Time (min)	Charge passed (C)	CO formed (μmol)	FE for CO (%)	CH_4 formed (nmol)	FE for CH_4 (%)
Cu foil	-1.0	30	0.199	ND	-	ND	-
	-1.0	60	0.271	ND	-	16.8	4.79
	-1.5	30	10.5	0.130	0.239	ND	-
	-1.5	60	17.1	0.502	0.566	10.0	0.0453
Cu-Ppy, 0.05 M	-1.0	30	2.03	0.028	0.266	5.05	0.192
	-1.0	60	3.82	0.0583	0.294	11.5	0.232
	-1.25	30	13.5	0.423	0.606	ND	-
	-1.25	60	27.1	0.798	0.568	ND	-
	-1.35	30	11.9	0.825	1.34	ND	-
	-1.35	60	23.1	1.34	1.12	ND	-
Cu-PPy, 0.1 M	-1.0	30	3.06	ND	-	ND	-
	-1.0	60	5.72	0.0153	0.0514	19.9	0.268
	-1.25	30	11.5	0.318	0.533	25.7	0.172
	-1.25	60	23.1	0.591	0.493	23.4	0.0782
Cu-Sn-Ppy, 0.2 M	-1.25	30	11.7	1.23	2.03	15.8	0.104
	-1.25	60	23.3	3.45[b]	2.87[b]	19.3	0.0642
Sn foil	-1.5	30	4.41	1.53	6.68	8.48	0.149
	-1.5	60	8.16	3.11	7.37	30.0	0.283
Sn-Ppy, 0.1 M	-1.5	30	7.40	4.37	11.4	ND	-
	-1.5	60	14.5	5.09[b]	6.80[b]	ND	-
Sn-Ppy, 0.2 M	-1.5	30	7.17	3.24	8.70	ND	-
	-1.5	60	14.5	4.57[b]	6.09[b]	ND	-

[a] Concentrations listed for metal-PPy films indicate the concentrations of the corresponding metal ions in the deposition solution from which they were prepared. [b] The upper limit of detection for the GC detector was surpassed, so these values represent a minimum observed.

Following initial electrolysis experiments a larger cell was designed and utilized due to the flaws of the original split cell design. The large cell, described in section 5.2.5, had more secure seals and more headspace (95.0 mL) for product accumulation. The increased volume prevented the product concentrations from exceeding the detection limit of the GC detector, and the improved seals prevented loss of product. An increased frit diameter in the large cell, 3 cm, decreased the resistance between the working and counter electrodes and allowed for more negative potentials to be analyzed than in the small cell. Greater emphasis was placed on studying the performance of the Sn-PPy films since they exhibited the greatest efficiencies for CO_2 reduction in the small cell.

As shown in Table 5.2, efficiency for CO production improved to 15.6% at -1.7 V vs Ag/AgCl for a Sn-PPy film, and C_2H_4, which was measured for this set of results, was observed at efficiencies as high as 7.71% at -1.25 V vs Ag/AgCl for a Sn-PPy film. CH_4 also represented a larger portion of the products measured, primarily for Sn-based electrodes, which was surprising since no CH_4 was observed for Sn-PPy electrodes in Table 5.1. All results shown in Tables 5.1 and 5.2 represent single sets of collected data as opposed to averages collected for multiple electrolysis trials, so more analysis would be needed in order to be statistically relevant and to identify outliers from typical performance.

Table 5.2. Results of electrochemical reduction of CO_2 in 0.1 M $KHCO_3$ (pH 6.8) at Cu, Cu-PPy, Sn, Sn-PPy, and Cu-Sn-PPy electrodes in a large split cell.

Electrode Material[a]	Potential (V vs Ag/AgCl)	Time (min)	Charge passed (C)	CO formed (μmol)	FE for CO (%)	CH_4 formed (μmol)	FE for CH_4 (%)	C_2H_4 formed (μmol)	FE for C_2H_4 (%)
Cu foil	-1.5	30	21.3	ND	-	ND	-	ND	-
	-1.5	60	39.7	0.475	0.231	ND	-	0.0806	0.235
Cu-PPy,	-1.5	30	23.5	2.50	2.06	0.226	0.742	ND	-
0.05 M	-1.5	60	47.6	4.67	1.90	0.213	0.346	0.129	0.314
Sn foil	-1.25	30	1.46	0.187	2.48	0.315	16.7	0.0299	2.38
	-1.25	60	2.76	ND	-	0.525	14.7	0.0152	0.636
	-1.5	30	3.54	2.18	11.9	0.700	15.3	0.0269	0.879
	-1.5	60	6.56	4.48	13.2	0.739	8.7	0.0896	1.58
	-1.75	30	9.1	1.07	2.27	ND	-	ND	-
	-1.75	60	17.5	3.13	3.46	0.220	0.973	ND	-
Sn-PPy, 0.1 M	-1.25	30	2.76	ND	-	ND	-	0.115	2.68
	-1.25	60	4.95	1.67	6.49	ND	-	0.330	7.71
	-1.5	30	5.25	2.70	9.94	ND	-	0.0575	1.27
	-1.5	60	10.9	4.70	8.30	0.0177	0.125	0.129	1.36
	-1.7	30	19.7	9.25	9.05	0.0925	0.363	0.0201	0.138
	-1.7	60	39.2	11.9	5.87	1.87	3.68	0.125	0.431
	-1.75	30	14	5.34	7.36	0.387	2.13	0.0425	0.352
	-1.75	60	28.6	11.9	8.04	2.69	7.25	0.0127	0.0516
Sn-PPy, 0.2 M	-1.7	30	17	11.5	13.0	1.80	8.16	0.160	1.09
	-1.7	60	35.6	28.7	15.6	0.291	0.631	0.146	0.474

[a] Concentrations listed for metal-PPy films indicate the concentrations of the corresponding metal ions in the deposition solution from which they were prepared.

5.4. Conclusion

While the CO_2 reduction results observed for Cu- and Sn-PPy films were low, they performed better than the corresponding metal foil electrodes in nearly every aspect. Unfortunately, the study was discontinued before a thorough analysis of CO_2 reduction on the metal-PPy films could be performed. Further optimization of the films, electrolyte concentration, potential, and reaction cell could lead to significant enhancements to CO_2 reduction performance. An improvement to CO production could make Sn-PPy films a viable material for syngas production, which is a mixture of CO and H_2 that can be converted into alcohols, or into hydrocarbons via the Fischer-Tropsch process.[1,3,4] Analysis of the liquid products and further analysis of gas products via gas chromatography-mass spectrometry (GC-MS) could identify addition CO_2 reduction products that were not detected using GC alone. Lastly, Cu-Sn-PPy films, which demonstrated high surface area morphologies and Cu-Sn alloy phases, would be of interest to study further to observed any possible synergistic CO_2 reduction effects.

5.5. References

1. S. C. Roy, O. K. Varghese, M. Paulose and C. A. Grimes, *ACS Nano*, 2010, **4**, 1259-1278.
2. G. A. Olah, G. K. S. Prakash and A. Goeppert, *J. Am. Chem. Soc.*, 2011, **133**, 12881-12898.
3. M. Mikkelsen, M. Jorgensen and F. C. Krebs, *Energy Environ. Sci.*, 2010, 3, 43-81.
4. D. T. Whipple and P. J. A. Kenis, J. *Phys. Chem. Lett.* 2010, **1**, 3451-3458.
5. E. B. Cole and A. B. Bocarsly, in *Carbon Dioxide as Chemical Feedstock, ed. M. Aresta*, Wiley, Weinheim, Germany, 1st edition, 2010, chapter 11, 291-316.
6. Y. Hori, A. Murata and R. Takahashi, *J. Chem. Soc., Faraday Trans. 1*, 1989, **85**, 2309-2326.
7. Y. Hori, I. Takahashi, O. Koga and N. Hoshi, *J. M. Catal. A: Chem*. 2003, **199**, 39 – 47.
8. K. P. Kuhl, E. R. Cave, D. N. Abram and T. F. Jaramillo, *Energy Environ. Sci.*, 2012, 5, 7050-7059.
9. M. Azuma, K. Hashimoto, M. Hiramoto, M. Watanabe and T. Sakata, *J. Electroanal. Chem.*, 1989, **260**, 441-445.
10. S. Nakagawa, A. Kudo, M. Azuma and T. Sakata, *J. Eletroanal. Chem.*, 1991, **308**, 339-343.
11. D. T. Whipple, E. C. Finke and P. J. A. Kenis, *Electrochem. Solid State Lett.*, 2010, **13**, B109-B111.
12. A. Dutta, M. Rahaman, M C. Luedi, M. Mohos and P. Broekmann, *ACS Catal.*, 2016, **6**, 3804-3814.

13. M. Watanabe, M. Shibata, A. Katoh, T. Sakata and M. Azuma, *J. Electroanal. Chem.*, 1991, **305**, 319-328.

14. N. Singh, PhD Thesis, Purdue University, 2010.

15. Y. Jung, N. Singh and K.-S. Choi, *Angew*. *Chem. Int. Ed.*, 2009, **48**, 8331 – 8334.